A remote sensing-based biophysical model for daily estimations of evapotranspiration and CO_2 uptake in high-energy water-limited environments

Deleted: approach

Deleted: using drought stress factor

David Helman[1,2,*], Itamar M Lensky[1], Yagil Osem[3], Shani Rohatyn[4], Eyal Rotenberg[4] and Dan Yakir[4]

[1] Department of Geography and Environment, Bar Ilan University, Ramat Gan 52900, Israel
[2] Department of Geography, University of Cambridge, Cambridge, CB2 3EN, UK
[3] Department of Natural Resources, Agricultural Research Organization, Volcani Center, Bet Dagan 50250, Israel
[4] Earth and Planetary Sciences, Weizmann Institute of Science, Rehovot 76100, Israel

[*]Corresponding author:
David Helman (dh565@cam.ac.uk ; davidhelman.biu@gmail.com)
Department of Geography, Bar-Ilan University, Ramat Gan 52900
Israel.
Tel: +972 3 5318342
Fax: +972 3 5344430

Abstract

Estimations of ecosystem-level evapotranspiration (ET) and CO_2 uptake in water-limited environments are scarce and scaling up ground-level measurements is not straightforward. A biophysical approach using remote sensing (RS) and meteorological data (RS-Met) is adjusted to extreme high-energy water-limited ecosystems that suffer from continuous stress conditions to provide daily estimations of ET and CO_2-uptake (measured as gross primary production – GPP) at a spatial resolution of 250-m. The RS-Met was adjusted using a seasonal water deficit factor (f_{WD}) based on daily rainfall, temperature and radiation data. We validated our adjusted RS-Met with eddy-covariance flux measurements using a newly developed mobile lab system and the single active Fluxnet station operating in this region (Yatir pine forest station) in a total of seven forest and non-forest sites across a climatic transect in Israel (280-770 mm y^{-1}). RS-Met was also compared to the satellite-borne Moderate Resolution Imaging Spectroradiometer (MODIS)-based ET and GPP products (MOD16 and MOD17, respectively) in these sites.

Results show that the inclusion of the f_{WD} significantly improved the model, with R=0.64-0.91 for the ET adjusted model (compared to 0.05-0.80 of the non-adjusted model) and R=0.72-0.92 for the adjusted GPP model (compared to R=0.56-0.90 of the non-adjusted model). The RS-Met (with the f_{WD}) successfully tracked observed changes in ET and GPP between dry and wet seasons across the sites. ET and GPP estimates from the adjusted RS-Met also agreed well with eddy covariance estimates at the annual timescale in the Fluxnet station of Yatir (266±61 vs. 257±58 mm y^{-1} and 765±112 vs. 748±124 gC m^{-2} y^{-1} for ET and GPP, respectively). Comparison with MODIS products showed consistently lower estimates from the MODIS-based models, particularly at the forest sites. Using the adjusted RS-Met, we show that afforestation significantly increased the water use efficiency (the ratio of carbon uptake to ET) in this region, with the positive effect decreasing when moving from dry to more humid environments, strengthening the importance of drylands afforestation. This simple but yet robust biophysical approach shows a promise for reliable ecosystem-level estimations of ET and CO_2 uptake in extreme high-energy water-limited environments.

Keywords: CO_2; ET; GPP; MODIS; NDVI; water deficit; water stress

Deleted: was previously proposed for ecosystem-level assessment relying on vegetation index and meteorological data (RS-Met) in temperate Mediterranean ecosystems. However, these RS-Met models have not been tested yet in extreme high-energy water-limited ecosystems that suffer from continuous stress conditions. Owing to the lack of ET and CO_2 flux estimations in the Eastern Mediterranean, we examined the RS-Met approach using

Moved (insertion) [2]

Deleted: .

Deleted: ,

Moved up [2]: in seven forest and non-forest sites across a climatic transect in Israel (280-770 mm y^{-1}).

Deleted: The RS-Met models were used with and without the addition of a seasonal drought stress factor (f_{DS}), which was based on daily rainfall, temperature and radiation data.

Deleted: the RS-Met models with the inclusion of the f_{DS} were

Deleted: compared to the non-f_{DS} models (

Deleted: r

Deleted: ;

Deleted: P=0.06 and r

Deleted: r

Deleted: ;

Deleted: P<0.01 for ET and GPP, respectively)

Deleted: These

Deleted: ,

Deleted: seasonal

Deleted: (ET_{MOD} = 0.94×ET_{EC} + 0.28; r=0.82; MAE=0.54 mm d^{-1}; N=243 d, and GPP_{MOD} = 0.99×GPP_{EC} + 0.51; r=0.86; MAE=1.03 gC m^{-2} d^{-1}; N=252 d)

Deleted: Modeled

Deleted: located in the dryland pine forest

Deleted: Using the RS-Met models, we were able to show the effect of afforestation on water vapor and CO_2 fluxes in this region. A

Deleted: was responsible for a

Deleted: in

Deleted: WUE

Deleted: This

Deleted: when adjusting for drought stress effects

Deleted: drought stress;

1. Introduction

Assessing the water use and carbon uptake in terrestrial ecosystems is important for monitoring biosphere responses to climate change (Ciais et al., 2005; Jung et al., 2010; Reichstein et al., 2013). Accurate estimations of evapotranspiration (ET) and gross primary production (GPP), as a measure of the CO_2 uptake, usually require the integration of extensive meteorological, flux and field-based data (e.g., Wang *et al.*, 2014; Kool *et al.*, 2014). However, scaling up field-based measurements to the ecosystem level is not straightforward and require the use of complex models (Way et al., 2015).

Currently, the eddy covariance (EC) technique is the most direct method for measuring carbon and water vapor fluxes at the ecosystem level (Baldocchi, 2003). The EC approach benefits from continuous temporal coverage; currently (April, 2017), there are more than 560 active EC sites across the globe, as part of the Fluxnet program (http://fluxnet.ornl.gov). However, there are also some practical and technical limitations. The EC measurement is representative of a relatively small area (<2 km^2), and the application of the EC approach is limited to relatively homogeneous and flat terrains. Additionally, most EC towers are concentrated in the US, Europe and Asia, with poor coverage in water-limited regions, such as North Africa and the Eastern Mediterranean (Schimel et al., 2015).

Remote-sensing-based models (RS models) have been used to overcome some of the limitations of EC, complementing the information derived from the flux towers. In contrast to process-driven models, RS models benefit from continuous, direct observation of the Earth's surface, acquiring data at a relatively high spatial resolution and with full regional to global coverage. Many RS models for the estimation of ET and GPP exist (see review in Kalma *et al.*, 2008), but these algorithms are too complex and most of the models are not provided as accessible products for researchers outside the remote sensing community. Particular exceptions are the satellite-borne Moderate Resolution Imaging Spectroradiometer (MODIS)-based ET and GPP products (MOD16 and MOD17), which provide 8-day ET and GPP estimates at 1-km for 2000-2015, globally (Mu et al., 2007, 2011, Running et al., 2000, 2004).

In the past decade, several simple biophysical ET and GPP models based on vegetation indices (from satellite data) have emerged, offering assessment at a relatively high-to-moderate spatial and temporal resolutions with an acceptable accuracy (i.e. daily estimates at 250 m; see e.g. Veroustraete *et al.*, 2002; Sims *et al.*, 2008; Maselli *et al.*, 2009, 2014; and

Deleted: of the utmost

Deleted: ce

Deleted: Measurements of leaf gas exchange and isotopic composition (e.g., δ^{13}C and δ^{18}O) have been used to estimate leaf-scale carbon and water fluxes (Klein et al., 2013; Maseyk et al., 2011; Raz-Yaseef et al., 2012a). Meanwhile, observations of sap flow and tree rings often serve to estimate fluxes at the tree-level (Klein et al., 2016; Wang et al., 2014).

Deleted: such

Deleted: most of them

Deleted: , with low accessibility

review of ET models in Glenn *et al.*, 2010). One of those models is the ET model based on the FAO-56 formulation (Allen et al., 1998). The FAO-56 formulation states that the actual ET of irrigated crops can be determined from the reference ET (ET_o) corrected with crop coefficient *Kc* values (see Eq. 2). The *Kc* varies mainly with specific plant species characteristics, which enables the transfer of standard *Kc* values among locations and environments (Allen et al., 2006).

The remote-sensing version of this formulation, uses a function of satellite-derived vegetation index, usually the normalized difference vegetation index (NDVI), as a substitute for the crop coefficient. Being a measure of the green plant biomass and the ecosystem leaf area, the NDVI is often used as a surrogate for plant transpiration and rainfall interception capacity (Glenn *et al.*, 2010). Additionally, the NDVI is closely related to the radiation absorbed by the plant and to its photosynthetic capacity (Gamon et al., 1995). However, the direct detection, through NDVI, of the abovementioned parameters at a seasonal timescale is still challenging and usually requires additional meteorological information (Helman et al., 2015a). The RS model based on the FAO-56 formulation combines the two sources of information, satellite and meteorological, providing a daily estimation of actual ET. This model, originally proposed for croplands and other managed vegetation systems (Allen et al., 1998; Glenn et al., 2010), was recently adjusted for applications in natural vegetation systems (Maselli *et al.*, 2014).

For the estimation of GPP, a simple but robust biophysical GPP model is the one based on the radiation use efficiency (RUE) model proposed by Monteith (1977). The classical Monteith-type model depends on the absorbed radiation and on the efficiency of the vegetation at converting this radiation into carbon-based compounds. Accordingly, this Monteith-based model is driven by radiation and temperature data, acquired from meteorological stations, and by the fraction of absorbed photosynthetically active radiation (*f*APAR), which can be calculated from the satellite-derived NDVI or EVI. A major challenge in this model, however, is the estimation of the RUE, a key component of the model, which usually depends on plant species type and environmental conditions. Currently, the conventional procedure is to use a plant-species-dependent maximum RUE from a lookup table and adjust it for seasonal changes using some sort of a factor that changes throughout the season based on meteorological data (Running et al., 2004; Zhao and Running, 2010).

Though simple, both ET and GPP models (hereafter RS-Met) were shown to be promising in accurately assessing daily ET and GPP at a relatively high spatial resolution (<1 km)

Deleted: see also the

Deleted: (Allen et al., 1998

Deleted: This

Deleted: model

Deleted: , which is defined as the ratio of the actual to the potential ET (ET_o) in the FAO-56 formulation

Deleted: by

Formatted: Font:Not Italic, Complex Script Font: Italic

Deleted: models

(Helman et al., 2017; Maselli et al., 2014, 2006; Veroustraete et al., 2002). However, the use of the RS-Met is limited to ecosystems under normally non-stressful conditions because there is no accurate representation of water availability in these models. Recently, the incorporation of a water-deficit factor (f_{WD}) in these models was proposed by Maselli *et al.*, (2009, 2014), adjusting for short-term stress conditions in water-limited natural ecosystems. The proposed f_{WD} is based only on daily rainfall data and daily potential ET calculated from temperature and/or incoming radiation. The RS-Met with the addition of the f_{WD} was successfully validated against EC-derived estimates of ET and GPP in several sites in Italy (Maselli et al., 2014, 2009, 2006).

Deleted: models
Deleted: drought
Deleted: stress
Deleted: f_{DS}
Deleted: f_{DS}
Deleted: models
Deleted: f_{DS}
Deleted: were

However, the RS-Met approach has never been tested in extreme high-energy water-limited environments such as those in the Eastern Mediterranean. Currently, there is only one active Fluxnet station in the entire Eastern Mediterranean (Yatir forest, southern Israel; Fig. 1a) that measures water vapor and carbon fluxes (since 2000); while in this region water is considered to be a valuable resource and the proper management of this resource depends on the accurate assessment of the ET component. Moreover, despite of the well-known important contribution of drylands regions to the global CO_2 (Ahlström et al., 2015), there are almost no efforts of estimating CO_2 fluxes in forested and non-forested areas in this dry region. This led to the development of the Weizmann mobile lab system (Israel; Fig. 1h) that allows extension of the permanent Fluxnet measurement sites on campaign basis (e.g., Asaf *et al.*, 2013; for technical detail see: http://www.weizmann.ac.il/EPS/Yakir/node/321). Such a system could allow flux and auxiliary analytical measurements across a range of climatic conditions, plant species and ecosystems, as well as addressing land use changes and disturbance. However, to extend these campaign-based measurements in time and space a model fitted to the high-energy water-limited conditions of this region is required.

Deleted: this

Here, we adjusted the RS-Met to the extreme hot and dry conditions of the Eastern Mediterranean region. The adjusted RS-Met was examined in a total of seven ecosystems distributed at three precipitation levels along a rainfall gradient (280-770 mm y^{-1}) in this region (Israel; Fig. 1). Ecosystems included three pairs of planted forests and adjacent non-forest sites (representing the original area on which these forests were planted). Ground-level campaign measurements of ET and net ecosystem CO_2 exchange using the newly developed mobile lab (Fig. 1h) and the continuous flux measurements in the active Fluxnet site in Yatir (Klein et al., 2016; Tatarinov et al., 2016) were used to validate the RS-Met. This combination of model-based estimates and direct flux measurements of ET and CO_2 uptake

Deleted: tested
Deleted: approach
Deleted: the Eastern Mediterranean
Deleted: models

across a range of climatic conditions and ecosystems provides a unique opportunity to test and validate the RS-Met approach in this high-energy water-limited region. Particularly, we examined the RS-Met with and without the application of the f_{WD}. We also compared the RS-Met with MODIS ET/GPP products in the studied sites.

Our specific goals in this study were to: (1) examine the seasonal evolution of the f_{WD} and its role in the RS-Met, (2) compare the model estimates with EC and MODIS ET/GPP products across these high-energy water-limited sites, at a daily and annual basis, and (3) use the RS-Met to estimate changes in water use efficiency (WUE=GPP/ET) following afforestation across the rainfall gradient in Israel, by comparing the three-paired forest vs. non-forest sites.

2. Materials and methods

2.1. Study sites

The sites in this study included three pairs of planted pine forests (*Pinus halepensis* Mill.) and adjacent non-forested (dwarf shrublands) sites distributed throughout a climatic range in Israel (P = 280 – 770 mm y^{-1}), from dry to sub-humid Mediterranean (Table 1 and Fig. 1a-f), which represent the typical Mediterranean vegetation systems in the Eastern Mediterranean. The three non-forested sites represent the original natural environment on which the pine forests were planted, while the afforested sites are currently managed by the Jewish National Fund (KKL). The non-forested shrubland sites are mostly dominated by *Sarcopoterium spinosum* (dwarf shrub) in a patchy distribution with a wide variety of herbaceous species, mostly annuals, growing in between the shrub patches during winter to early spring. In addition, we tested the models in one native deciduous forest site dominated by *Quercus* species. A brief description of the sites is given in the following:

Yatir. The forest of Yatir is an Aleppo pine forest (*Pinus halepensis*) that was planted by KKL mostly during 1964-1969 in the semiarid region of Israel (31.34N, 35.05E; Fig. 1a). It covers a total area of *c.* 2800 ha and lies on a predominantly light brown Rendzinas soil (79 ± 45.7 cm deep), overlying a chalk and limestone bedrock (Llusia et al., 2016). The average elevation is 650 m. The mean annual rainfall in the forest area is 285 mm y^{-1} (for the last 40 years) and was 279 mm y^{-1} in the Fluxnet site during 2001-2015 (Table 1). The mean annual temperature in Yatir is 18.2 °C with 13 and 31 °C for mean winter (November– January) and summer (May–July) temperatures, respectively. Tree density in Yatir is *c.* 300 trees ha^{-1} (Rotenberg and Yakir, 2011) with a tree average height of *c.* 10 m and canopy leaf area index

Deleted: models
Deleted: f_{DS}
Deleted: , which was originally proposed by Maselli *et al.* (2014) for temperate Mediterranean environments
Deleted: Thus, o
Deleted: f_{DS}
Deleted: estimation of the fluxes from the
Deleted: models in these environments
Deleted: measurements
Deleted: scale
Deleted: , with and without the use of the f_{DS}
Deleted: best
Deleted: models

(LAI) of 1.4 ± 0.4 m^2 m^{-2}, which displays small fluctuations between winter and summer (Sprintsin et al., 2011). The understory in this forest is mostly comprised of ephemeral herbaceous species (*i.e.*, theropytes, geophytes and hemicryptophytes) growing during the wet season (September-April) and drying out in the beginning of the dry season (May-June). A relatively thin needle litter layer covers the forest floor during the needle senescence period (June-August) (Maseyk et al., 2008).

Eshtaol. The forest of Eshtaol was planted in the late 1950's by KKL with mostly *P. halepensis* trees in the central part of Israel (31.79N, 34.99E; Fig. 1c). The current forest area is *c.* 1200 ha and lies mainly on Rendzinas soils. The average elevation is 330 m. The mean annual rainfall in this area is *c.* 500 mm y^{-1} and was a 480 mm y^{-1} in the site of the EC measurements during 2012-2015 (Table 1). Tree density in Eshtaol is typically 300–350 trees ha^{-1}, with a tree canopy LAI that ranges between 1.9 m^2 m^{-2} and 2.6 m^2 m^{-2} and a tree average height of 12.5 m (Osem et al., 2012).

Birya. The forest of Birya is a *P. halepensis* forest that was mostly planted during the early 1950's in the northern part of Israel, Galilee region (33.00N, 35.48E; Fig. 1e). The forest covers an area of *c.* 2100 ha and lies on a Rendzinas and Terra rossa soils. The average elevation is 730 m. The average temperature in this area is 16°C, with an average annual rainfall of 710 mm y^{-1} and 776 mm y^{-1} during the years of the EC measurements (2012-2015; Table 1). The average stand density is 375 trees ha^{-1} with an average tree height of 11 m (Llusia et al., 2016).

HaSolelim. The HaSolelim forest is a native deciduous mixed oak forest dominated by *Quercus ithaburensis*, which is accompanied by *Quercus calliprinos* (evergreen) and few other Mediterranean broadleaved tree and shrub species (Fig. 1g). The forest is located at the northern part of Israel in the Galilee region, 30 km south of the Birya forest (32.74N, 35.23E). The forest covers an area of *c.* 240 ha and lies on Rendzinas and Terra rossa soils. The elevation in the site of the EC measurements is 180 m (Table 1). The average temperature in this area is a typically 21°C, with a mean annual rainfall of 580 mm y^{-1} and 543 mm during the years of the EC measurements. The site where the measurements took place is characterized by an average stand density of 280 trees ha^{-1} and an average tree height of 8 m (Llusia et al., 2016).

Wady Attir. This is a xeric shrubland site located southwest to the forest of Yatir (31.33N, 34.99E). The average elevation is 490 m. The site is dominated by semi-shrubs species such as, *Phagnalon rupestre* L, with *graminae* species, mainly *Stipa capensis* L. (also known as Mediterranean needle grass), *Hordeum spontaneum* K. Koc. (also known as wild barley) and some *Avena* species such as, *A. barbata* L. and *A. sterilis* L., appearing shortly after the rainy season (Leu et al. 2014; Fig. 1b). The mean annual rainfall in this area is 230 mm y^{-1} (Mussery et al., 2016) and was 280 mm y^{-1} in the years of the EC measurements (2012-2015; Table 1).

Modiin. The shrubland site of Modiin is located few kilometers from the forest site of Eshtaol and represent the original environment on which this forest was planted (31.87N, 35.01E; Fig. 1d). The average elevation is 245 m. The shrubland site is mostly dominated by *Sarcopoterium spinosum* (dwarf shrub) in a patchy distribution with a wide variety of herbaceous species, mostly annuals, growing in between the shrub patches during winter to early spring. The average rainfall amount in this area was 480 mm y^{-1} in the years of the EC measurements (Table 1).

Kadita. The shrubland site of Kadita is also dominated by *Sarcopoterium spinosum* (dwarf shrub) in a typical patchy distribution (Fig. 1f). It is located nearby the forest of Birya at an elevation of 815 m (33.01N, 35.46E; Table 1). The mean annual rainfall in this site is similar to that recorded in the Birya forest (i.e., 766 mm y^{-1} in the years of study).

All shrubland sites have been under continuous livestock grazing for many years, and their vegetation structures are mainly the outcome of both rainfall amount and grazing regime.

2.2. Satellite-derived vegetation index

We used the NDVI from the moderate-resolution imaging spectroradiometer (MODIS) on board NASA's Terra satellite at 250 m spatial resolution (MOD13Q1). The MOD13Q1 NDVI product is a composite of a single day's value selected from 16-day periods based on the maximum value criteria (Huete et al., 2002). The Terra's NDVI product is acquired during the morning (10:30 am) and thus provides a good representation of the peak time of the plants' diurnal activity. The gradual growth of the vegetation enables the interpolation of the 16-day NDVI time series to representative daily values (Glenn et al., 2008; Maselli et al., 2014). We downloaded the 16-day NDVI time series covering the main area of the eddy covariance flux measurement for each site from the MODIS Subsets (http://daacmodis.ornl.gov/cgi-bin/MODIS/GLBVIZ_1_Glb/modis_subset_order_global_col5.pl) for the period October 2001 – October 2015. Then, we pre-processed the NDVI time series as described in Helman et al. (2014a, 2014b, 2015b) to remove outliers and uncertainties due to cloud contamination and atmospheric disturbances without removing important information (see Fig. S2). The processed 16-day NDVI time series were then interpolated on a daily basis using the local scatterplot smoothing technique (LOESS). This technique is suited for eliminating outliers in non-parametric time series and has been shown to be a useful tool in the interpolation of datasets with a seasonal component (Cleveland, 1979).

2.3. The mobile lab system and the Fluxnet station in Yatir

A newly designed mobile flux measurement system was used in all campaigns (Fig. 1h), based on the 28-m pneumatic mast on a 12-ton 4x4 truck that included a laboratory providing an air-conditioned instrument facility (cellular communication, 18 KVA generator, 4200 WUPS). Flux, meteorological and radiation measurements relied on an eddy-covariance system that provides CO_2 measurements and sensible and latent heat fluxes using a three-dimensional sonic anemometer (R3, Gill Instruments, Lymington, Hampshire, UK) and enclosed-path CO_2-H_2O IRGA (Licor 7200, Li-Cor, Lincoln, NE, USA) using CarboEuroFlux methodology (Aubinet et al., 2000), and EddyPro Software (www.licor.com). Data were collected using self-designed program in LabVIEW software. Air temperature and relative humidity (HMP45C probes, Campbell Scientific) and air pressure (Campbell Scientific sensors) were measured at 3 m above the canopy. Energy fluxes relied on radiation sensors, including solar radiation (CMP21, Kipp and Zonen), long-wave radiation (CRG4, Kipp and Zonen) and photosynthetic radiation (PAR, PAR-LITE2) sensors. All sensors were installed in pairs facing both up and down and are connected using the differential mode through a multiplexer to a data logger (Campbell Scientific). GPP for each site was calculated from the measured net ecosystem CO_2 exchange (NEE) after estimating ecosystem respiration, Re, and using the regression of NEE on turbulent nights against temperature, followed by extrapolating the derived night-time Re-temperature relationship to daytime periods (Reichstein *et al.*, 2005; modified for our region by Afik, 2009). Flux measurements with the mobile system were carried out on a campaign basis, in six of the seven sites, with each campaign representing approximately two weeks in a single site, repeated along the seasonal cycle with mostly two but sometimes only one two-weeks set of measurements per cycle, during the 4 years of measurements, 2012-2015. Continuous flux measurements were carried out in the permanent Fluxnet site of Yatir (xeric forest site). Begun in 2000, the eddy covariance (EC) and supplementary meteorological measurements have been conducted continuously (Rotenberg and Yakir, 2011; Tatarinov et al., 2016), with measurements

Deleted: estimated

Deleted: using the conventional approach of

Deleted: a

performed according to the Euroflux methodology. Instrumentation is similar to that in the Mobile Lab except for the use of a closed-path CO_2/H_2O infrared gas analyzer (IRGA, LI-7000; Li-Cor, Lincoln, NE) with the inlet placed 18.7 m above ground. Typical fetch providing 70% (cumulative) contribution to turbulent fluxes was measured between 100 m and 250 m (depending on the site) along the wind distance. This was taken in consideration when using the MOD13Q1 product to derive the modeled fluxes.

During April 2012, at the peak activity season in Yatir forest, the mobile lab system for two weeks deployed at 10 m distance away from the permanent flux measurements tower, were both EC systems measuring at the same height and fluxes calculated by the same software (EddyPro 3.0 version; Li-Cor, USA). The linear correlation (R^2) and the slope of the Mobile Lab measured fluxes of H, LE and NEE *vs.* the permanent Tower fluxes were 0.9 and 1.0 for H, 0.8 and 0.9 for LE and 0.9 and 1 for NEE, respectively.

Daily estimates of reference evapotranspiration, i.e. ET_o (in mm d^{-1}), for the ET model, the water deficit and the water availability factors, were calculated from the mean daily air temperature and the daily total incoming solar radiation, measured at the seven sites following the empirical formulation proposed by Jensen & Haise (1963):

Deleted: potential

Deleted: drought

Deleted: stress

Deleted: factor

$$ET_o = \frac{R_g}{2470}(0.078 + 0.0252\ T) \qquad (1)$$

where T is the mean daily air temperature (in °C), and R_g is the daily global (total) incoming solar radiation (in kJ m^{-2} d^{-1}); ET_o is finally converted into mm d^{-1} by dividing the R_g by 2470 mm kJ m^{-2} d^{-1} (see in Jensen & Haise, 1963). We decided to use this ET_o formulation of Jensen & Haise (1963) to be consistent with the original RS-Met proposed by Maselli et al. (2014) though we are aware of the large tradition of works devoted to compare several methods to estimate ET_o, and to prove the validity and limitations of these methods under different environmental conditions.

2.4. MODIS ET/GPP products and the PaVI-E model for annual ET

Deleted: *The*

We compared our RS-Met with the products from MODIS-based ET and GPP models, which details of these models can be found in Mu et al. (2007, 2011) and Running et al. (2000, 2004) for the ET and GPP models, respectively. These products (MOD16 and MOD17 for ET and GPP, respectively) provide 8-day ET and GPP estimates at 1-km for 2000-2015, globally. MODIS ET/GPP products were compared with RS-Met at the seasonal and annual scale in all sites. Importantly, these MODIS products take advantage of the use of vapor pressure information, which was shown to affect the stomatal conductance of plants whereas our model did not consider this factor directly. We did not use vapor pressure data in the RS-Met because most of the weather stations in this region do not have such information and that would have limited the use of our model. However, the f_{WD} calculated from radiation, temperature and water supply (rainfall) data, is used in the adjusted RS-Met as an indirect proxy for VPD. To compare with the 8-day MODIS ET/GPP products we averaged the daily RS-Met and EC estimates over the same 8-day periods.

We also compared the RS-Met ET estimates to the annual ET derived from PaVI-E (Parameterization of Vegetation Index for the estimation of ET model; Helman et al., 2015a) at the six sites on an annual basis. The PaVI-E is an empirical model based on simple exponential relationships found between MODIS-derived EVI (and NDVI) and annual ET estimates from EC in 16 Fluxnet sites, comprising a wide range of plant functional types across Mediterranean-climate regions. This simple relationship (PaVI-E) was shown to produce accurate ET estimates at the annual timescale (mm y^{-1}) and at a moderate spatial resolution of 250 m in this region (Helman et al., 2015a). It was validated against physical-based models (MOD16 and MSG LSA-SAF ETa) and ET calculated from water balances across the same study area. PaVI-E was used for ecohydrological studies in this region, providing insights into the role of climate in altering forest water and carbon cycles (Helman et al., 2017, 2016). The advantage of this model, is that it does not requires any additional meteorological information but is a proper function of the relationship between observed fluxes and satellite-derived vegetation indices. This makes it interesting to compare with the RS-Met model since the RS-Met is highly dependent on meteorological forcing.

3. Description of the models and the use of a water deficit factor

The RS-Met models used here for the daily estimation of ET and GPP are based on the NDVI and the meteorological data. Each model was applied with and without a water deficit factor (f_{WD}) adjustment (i.e., two model versions for ET and two for the GPP).

3.1. The ET model

The RS-Met of daily ET is based on the FAO-56 formulation (Eq. 2):

$$\mathrm{ET} = \mathrm{ET_o} \times (K_C + K_S) \qquad (2)$$

Deleted: used
Deleted: the
Deleted: model
Deleted: to validate the ET from the RS-Met model on an annual basis
Deleted: owing to the lack of continuous flux measurements in
Deleted: of the seven
Deleted: (Eshtaol, HaSolelim, Birya, Wady Attir, Modiin and Kadita, see Table 2 for N of the EC flux measurements in each of those sites)
Deleted: the
Deleted: measured
Deleted: with
Deleted: The PaVI-E model produces annual ET at a spatial resolution of 250 m and
Deleted: retrieved
Deleted: (Helman et al., 2015a)
Deleted: It
Deleted: shown to be useful
Deleted: study
Deleted: PaVI-E
Deleted: alone
Deleted: drought
Deleted: stress
Formatted: Space After: 12 pt
Deleted: (Maselli et al., 2014, 2009, 2006; Veroustraete et al., 2002)
Deleted: (DS)
Deleted: (no-DS)
Deleted: drought
Deleted: stress
Deleted: s
Deleted: model

Where K_C and K_S stand for the crop/canopy and soil coefficients, respectively (Allen et al., 1998). In the RS-Met a maximum value of K_C (K_{C_max}), which depends on the type of the monitored vegetation (Allen et al., 1998; Allen et al., 2006), and a maximum value of K_S (K_{S_max}), for soil evaporation, are used as a reference in the model. The K_{C_max} and K_{S_max} are then multiplied by a linear transformation of the NDVI (i.e., f(NDVI) and f(1-NDVI), respectively, Maselli et al., 2014) to adjust for the seasonal evolution of the crop/canopy and soil coefficients:

Deleted: model

$$K_C = K_{C\_max} \times f(\text{NDVI}) \qquad (3)$$

$$K_S = K_{S\_max} \times f(1\text{-NDVI}) \qquad (4)$$

The linear transformation of the NDVI used here is the fractional vegetation cover (fVC) that better represent both ET processes: direct soil evaporation and plant transpiration. The fVC is a classical two-end member function based on minimum and maximum values of NDVI, corresponding to a typical soil background without vegetation ($NDVI_{SOIL}$) and an area fully covered by vegetation ($NDVI_{VEG}$), respectively:

Deleted: Following Maselli *et al.* (2014), we

Deleted: to

$$fVC = (\text{NDVI} - \text{NDVI}_{SOIL}) / (\text{NDVI}_{VEG} - \text{NDVI}_{SOIL}) \qquad (5)$$

Thus, Eqs. (3) and (4) become:

$$K_C = K_{C\_max} \times fVC \qquad (6)$$

and

$$K_S = K_{S\_max} \times (1 - fVC), \qquad (7)$$

respectively.

The fVC in Eq. (5) is calculated on a daily basis from the interpolated NDVI (daily) data. Note that the fVC in Eq. (6) represents the fraction of the area covered by the vegetation, while in Eq. (7) the term 1- fVC represents the fraction of the bare soil area. Both terms, fVC and 1-fVC in Eqs. (6) and (7), change over the course of a year due to canopy development and/or the appearance of ephemeral herbaceous plants. We used here the values of 0.1 and 0.8 for the $NDVI_{SOIL}$ and $NDVI_{VEG}$, respectively, which are the values observed for bare ground and dense natural vegetation in this region (Helman et al., 2015b).

Finally, from Eqs. (2) and (5-7) we obtain the model without the water deficit factor adjustment (NO f_{WD}):

$$ET = ET_o \times \{[fVC \times K_{C\_max}] + [(1\text{-}fVC) \times K_{S\_max}]\} \quad (8)$$

Following, we used a water deficit (f_{WD}) and water availability (f_{WA}) factors to adjust the crop/canopy and soil coefficients for water supply conditions at the root-zone and top-soil, respectively, in Eqs. (6) and (7):

$$K_C = K_{C\_max} \times fVC \times f_{WD} \quad (9)$$

and

$$K_S = K_{S\_max} \times (1\text{-}fVC) \times f_{WA} \quad (10)$$

The f_{WD} and f_{WA} in Eqs. (9) and (10) simulate the effects of available water for plant transpiration at the root zone and for surface evaporation at the top-soil, respectively, whereas the f_{WD} is defined as follows:

$$f_{WD} = 0.5 + 0.5 \times f_{WA} \quad (11)$$

The water availability factor (f_{WA}) is calculated as the simple ratio between the daily rainfall amount and the daily ET_o, both cumulated over a period of two months. Basically, the accumulation period could vary for different ecosystem types and environmental conditions. However, we have taken here a period of two months for the native shrublands and planted (and native) forests following previous observations that showed that this period is sufficient to maintain wet the topsoil layer for the whole rainy season in ecosystems in this region (Raz-Yaseef et al. 2010; 2012). Furthermore, changing the accumulation period did not gave us a consistently better results in all sites, as the two-month period gave us.

Deleted: as proposed in
Deleted: for this region
Deleted: drought stress
Deleted: no-
Deleted: DS
Deleted: Maselli *et al.* (2014)
Deleted: drought stress
Deleted: factor
Deleted: f_{DS}
Deleted: and the
Deleted: (f_{WA})
Deleted: stressful
Deleted: , respectively
Deleted: f_{DS}
Deleted: f_{DS}
Deleted: drought
Deleted: stress
Deleted: and available water (or water shortage)
Deleted: for plant transpiration and bare soil evaporation
Deleted: f_{DS}
Deleted: is
Deleted: f_{DS}
Formatted: Space After: 6 pt
Deleted: (Maselli *et al.*, 2014)
Moved (insertion) [1]
Deleted: Maselli et al. (2014) that suggested the use of a longer period (two months) for such ecosystems compared to the short period (one month) often used for annual crops.
Deleted: of

The f_{WA} is set to 1 when the cumulated rainfall amount exceeds the atmospheric demand (i.e., the ET_o). Note that the f_{WD} would then vary between 0.5 and 1, meaning that ET is reduced to half the potential maximum in the absence of water supply, simulating the basic transpiration levels maintained by evergreen vegetation (Glenn et al., 2011; Maselli et al. 2014). This reduction in the f_{WD} accounts for water deficit at the root zone, which results in reduced plant transpiration, while short-term effects would be mainly reflected through changes in the NDVI (and consequently in the *fVC* and *f*APAR; Glenn et al., 2010; Running and Nemani, 1988). In contrast to the f_{WD}, the f_{WA} is reduced to zero following a dry period longer than two months, making the surface evaporation component null during the dry summer.

The model is adjusted to root-zone and surface water deficit conditions (f_{WD} and f_{WA}) by replacing Eqs. (6) and (7) by Eqs. (9) and (10):

$$ET = ET_o \times \{[fVC \times K_{C\_max} \times f_{WD}] + [(1\text{-}fVC) \times K_{S\_max} \times f_{WA}]\} \quad (12)$$

Here we used a K_{C_max} value of 0.7 for both forests and non-forest sites, and a K_{S_max} value of 0.2 for soil evaporation in both (adjusted and unadjusted for water deficit conditions) models, as in Maselli et al., (2014).

Finally, the model derives daily ET estimates (in mm d^{-1}) at the spatial resolution of the MODIS NDVI product, i.e., 250 m.

3.2. The GPP model

For the GPP model, we used the biophysical radiation use efficiency model proposed by Monteith (1977):

$$GPP = RUE \times fAPAR \times PAR \quad (13)$$

where PAR is the daily incident photosynthetic active radiation (in MJ m^{-2}), calculated as 45.7% from the incoming measured global solar radiation (Nagaraja Rao, 1984), and *f*APAR is the fraction of the PAR that is actually absorbed by the canopy (range from 0 to 1). The *f*APAR was derived here from the daily NDVI time series following the linear formulation: *f*APAR = 1.1638 NDVI – 0.1426, which was proposed by Myneni & Williams (1994). This linear formulation was successfully applied in similar remote-sensing-based GPP models for similar ecosystems by Veroustraete *et al.* (2002), Maselli *et al.* (2006, 2009) and Helman *et*

Deleted: on

Deleted: f_{DS}

Moved up [1]: Basically, the accumulation period could vary for different ecosystem types. However, we have taken here a period of two months for the native shrublands and planted (and native) forests following Maselli et al. (2014) that suggested the use of a longer period (two months) for such ecosystems compared to the short period (one month) often used for annual crops.

Deleted: DS

Deleted: Replacing

Deleted: the no-DS model (Eq. 8) becomes the following DS model

Deleted: f_{DS}

Formatted: Space After: 6 pt

Deleted: DS and no-DS

Deleted: previously proposed by

Deleted: for similar woody-dominated ecosystems

Deleted: both

Deleted: the DS (Eq. 12) and no-DS (Eq. 8) models

Deleted: *f*PAR

Deleted: following

Deleted:),

Deleted: which

Deleted: and

al. (2017); RUE is the radiation use efficiency (in g C MJ^{-1}), which is the efficiency of the plant for converting the absorbed radiation into carbon-based compounds and which changes over the course of a year (Garbulsky et al., 2008).

The RUE is an important component in the GPP model and is the most challenging parameter to compute. It is usually considered to be related to vapor pressure deficit, water availability, temperature and plant species type (Running et al., 2000), and there have been several recent efforts to directly relate it to the photochemical reflectance index (PRI), which can also be derived from satellites (Garbulsky et al., 2014; Peñuelas et al., 2011; Wu et al., 2015). Currently, the conventional modeling of RUE for Mediterranean ecosystems is not straightforward and is mostly site specific, derived for specific local conditions (Garbulsky et al., 2008). Here, we used the simple approach proposed by Veroustraete *et al.*, (2002) and further developed by Maselli *et al.*, (2009), which states that a potential RUE (RUE_{MAX} in g C MJ^{-1}) can be adjusted for seasonal changes using a function based on temperature and water deficit conditions (f_{WT}):

Deleted: stress

$$RUE = RUE_{MAX} \times f_{WT} \quad (14)$$

The f_{WT} adjusts the RUE_{MAX} for seasonal changes following changes in water availability and temperature conditions:

$$f_{WT} = T_{CORR} \times f_{WD} \quad (15)$$

Deleted: f_{DS}

where T_{CORR} is a temperature correction factor calculated on a daily basis (Veroustraete et al., 2002):

$$T_{CORR} = \frac{e^{\left(a - \frac{\Delta H_{AP}}{G \cdot T}\right)}}{1 + e^{\left(\frac{\Delta S \cdot T - \Delta H_{DP}}{G \cdot T}\right)}} \quad (16)$$

where *a* is a constant equal to 21.9; ΔH_{AP} and ΔH_{DP} are the activation and deactivation energies (in J mol^{-1}), equal to 52750 and 211, respectively; G is the gas constant, equal to 8.31 J K^{-1} mol^{-1}; ΔS is the entropy of the denaturation of CO_2 and is equal to 710 J K^{-1} mol^{-1}; and T is the mean daily air temperature (in Kelvin degrees); and f_{WD} is the same water-deficit factor as in Eq. (11).

Deleted: f_{DS}

Deleted: drought

Deleted: stress

The water deficit factor, f_{WD}, is used here only in the model that considers water supply conditions. Thus, in the model without the f_{WD}, the f_{WT} would be only a function of the temperature, and thus $f_{WT} = T_{CORR}$ (in Eq. 15). Following Garbulsky *et al.*, (2008) and Maselli *et al.*, (2009), a constant value of 1.4 g C MJ^{-1} was used here for RUE_{MAX} in all sites and model variations (i.e., with and without the f_{WD}). The exclusion of direct measurements of vapor pressure deficit (VPD) as an input in the model is indeed a limitation; however, we tried to maintain a model with minimal input data that will be available from standard weather stations (VPD information is currently lacking from most of the weather stations in this region). The inclusion of the f_{WD}, which includes radiation, temperature and water supply (rainfall) information is used as an indirect proxy for VPD in the model.

Deleted: drought stress
Deleted: f_{DS}
Deleted: DS
Deleted: (i.e., the model
Deleted: drought
Deleted: stress
Deleted:)
Deleted: no-DS
Deleted: s
Deleted: the DS and no-DS

Finally, daily GPP values were computed from the model at a spatial resolution of 250 m for each of the seven sites and compared with EC estimates and the MODIS GPP product. It should be stated that the use of the EC-derived GPP as a reference in the validation should be taken with caution because GPP by itself is modeled and not directly measured. This may introduce uncertainties to the validation that could be contaminated by self-correlation.

Deleted: both the DS and no-DS
Deleted: s,
Deleted: the
Deleted: measurements

4. Testing the water deficit factor in high-energy water-limited environments

To show the importance of the water deficit factor (f_{WD}) in adjusting the model to seasonal variations in the fluxes, we demonstrate the seasonal evolution of the f_{WD} together with that of the main drivers of the RS-Met at the dryland pine forest site of Yatir (Fig. 2). Figure 2a shows that the f_{WD} moderate the increase of K_C (blue line in middle panel of Fig. 2a) at the beginning of the rainy season (November-January) even though the *fVC* (green line in lower panel of Fig. 2a) is relatively high likely due to the appearance of ephemeral herbaceous vegetation in the forest understory (Helman et al., 2015b). This is a realistic scheme since the herbaceous vegetation has little contribution to the ecosystem fluxes but a significant contribution to the NDVI (and thus to the *fVC*) signal (Helman, n.d.), as observed by the low EC GPP at this time (red dots in lower panel of Fig. 2a). Thus, the f_{WD} has an important role in reducing the K_C to a more realistic low values at this stage of the year when there is less water available for the trees. The same applies for the end of the rainy season and summer, in May-August, when the ET_o is relatively high but there is almost no available water for ET, as implied from the low f_{WD} (black line in upper panel of Fig. 2a).

Deleted: drought stress
Deleted: f_{DS}
Deleted: tracking the
Deleted: at high-energy water-limited environments
Deleted: f_{DS}
Deleted: components
Deleted: models
Deleted: one
Deleted: selective
Deleted: f_{DS}
Deleted: in the forest site of Eshtaol
Deleted: October
Deleted: December
Deleted: f_{DS}
Deleted: (Fig. 2a)
Deleted: April
Deleted: May
Deleted: both
Deleted: and the *fVC* are

In the GPP model, the f_{WD} reduces the high RUE at both ends of the rainy season, adjusting the GPP to the water deficit conditions at the root-zone during these periods (Fig. 2b). Here

Deleted: f_{DS}
Deleted: f_{DS}
Deleted: stress

again, the low f_{WD} reduces the contribution of the high fAPAR (and the RUE) in the model during the start of the rainy season due to the growth of ephemeral plants in the understory (green and blue lines in lower and middle panels of Fig. 2b, respectively). This is because there is still not sufficient water in the root-zone during this period. Particularly noted, though, is the significant reduction in GPP at the end of the rainy season and during the summer (May-August), when the PAR (yellow line in lower panel of Fig. 2b) is high but less water is available for transpiration and subsequently for photosynthesis.

Deleted: April
Deleted: May
Deleted: both
Deleted: and the RUE are

5. Comparisons with MODIS and the Fluxnet station in Yatir

5.1. Daily ET and GPP

We compared the daily estimates of the modeled ET with MODIS ET/GPP products and the active Fluxnet station at the dryland pine forest of Yatir for 2002-2012 (Table 1). As expected from the noted above (Section 4), the model without the water deficit factor (NO f_{WD} in Fig. 3a and 3e) overestimated the ET in comparison to the eddy covariance measurements, particularly from mid spring to the end of the summer (Fig. 3a,e). The peak ET was shifted to late July – early September, while the ET measured from the eddy covariance showed an earlier peak, in March. The large overestimation of the model without the f_{WD} was associated with the high ET_o during the spring and summer (R=0.91; P<0.001; see also Fig. 2a), which is the driver of the ET model (Eqs. 2, 8 and 12), following the low humidity and augmented radiation load at this time of the year (Fig. 2 and Rotenberg and Yakir, 2011; Tatarinov et al., 2016). However, including the f_{WD} in the model helped to correct for this overestimation, by linking ET to the available soil water (Fig. 2a), resulting in a good agreement between the model and the eddy covariance estimates (Fig. 3c and 3e; Table 2).

Deleted: drought stress
Deleted: no-DS
Deleted: (Fig. 3a and 3e)
Deleted: no-DS
Deleted: r
Deleted: drought
Deleted: stress and the available water
Deleted: factors

When comparing the modeled GPP with the EC estimates at Yatir, the model without the f_{WD} (NO f_{WD} in Fig. 3b and 3f) produced higher values during both ends of the rainy season (October-November and May-June). In particular, the model without the f_{WD} overestimated the GPP during the start of the rainy season (indicated by the arrows in Fig. 3b). This was likely due to the increase in the NDVI following the appearance of ephemeral herbaceous plants in the understory of these Mediterranean forests in the beginning of the rainy season, as already pointed out in the previous section (see also Helman et al., 2015b). The herbaceous vegetation in the understory of Yatir provides a meaningful contribution to the NDVI signal,

Deleted: drought stress factor
Deleted: no
Deleted: -
Deleted: DS
Deleted: , Fig. 3b and 3f
Deleted: no-DS
Deleted: vegetation
Deleted: Also here, t

although it constitutes only a minor component in terms of the biomass and the CO_2 uptake of the forest (Helman et al., 2015b; Rotenberg and Yakir, 2011). Considering f_{WD} in the model thus abridged the RUE, counterbalancing the high contribution of the herbaceous vegetation to the *f*APAR through the high NDVI. This also better simulated the water deficit conditions experienced by the woody vegetation, which is the main contributor to the GPP in Yatir, during the dry period (Fig. 3d and 3f).

These results explicitly show that the water deficit factor is useful in “forcing” the model onto the woody vegetation activities (strongly restricted by water shortage at both ends of the rainy season), reducing the impact of other components, such as the peak activities of the understory vegetation that, obviously, does not suffer from water shortage and responds to small early season moisture input (Helman et al., 2014a, n.d.; Mussery et al., 2016).

Comparison with MODIS ET/GPP products show a consistent underestimation of the fluxes at the peak season and overestimation at the dry season, implying that these models need to be adjusted to root-zone water deficit conditions in such high-energy water-limited sites (Fig. 4). This is in spite of the use of vapor pressure data in these models (Mu et al., 2007, 2011, Running et al., 2000, 2004). These results suggest that including the f_{WD} in global models, such as the MODIS-based models, might at least reduce the observed dry period overestimations and increase fluxes at the wet season.

5.2. Annual-basis comparisons

We then examined the adjusted RS-Met on an annual scale, first by comparing the inter-annual variation in the modeled ET with that from the EC and with that from the MODIS ET product at Yatir (Fig. 5a). This analysis indicated that RS-Met can also reproduce the annual ET with a fair accuracy, showing a moderate but significant correlation with the total annual ET derived from the daily summed EC estimates (R=0.78; P<0.05; N=10; Fig. 5b) and comparable mean annual ET (266±61 vs. 257±58 mm y^{-1} for ET_{MOD} and ET_{EC}, respectively). MODIS ET, in turn, was not correlated with EC (R=0.10; P>0.1; N=11) showing little year-to-year variations in the annual ET (Fig. 5a,c).

Both the RS-Met and the EC were significantly correlated with P (R=0.60 and 0.93; P=0.05 and <0.001, respectively), showing similar patterns in water use (ET/P ratio), though differing in magnitude in some of the years studied (black and red lines in upper panel of Fig. 5a and Fig. S3). The little year-to-year variation in the MODIS ET resulted in a noisier pattern of water use (green line in upper panel of Fig. 5a) compared to that calculated from

Deleted: the drought stress factor
Deleted: RS-Met
Deleted: P
Deleted: drought stress
Deleted: drought stress
Deleted: focusing
Deleted: RS
Deleted: data
Deleted: model with the drought-stress factor (DS model)
Deleted: , as well as with the annual rainfall (P)
Deleted: this
Deleted: site
Deleted: 4a
Deleted: the
Deleted: model
Deleted: r
Deleted: 4b
Deleted: r
Deleted: Fig. 4a

the RS-Met and EC. A noisy water use pattern was also noted in the RS-Met (compared to that from the EC), particularly in dry years (Fig. S3; e.g., 2003, 2005 and 2008; Fig. 5a). Higher ET in the RS-Met was likely the result of discrepancies in daily estimates during the summer between the RS-Met and EC (R=0.05; P>0.1 for June-August; Fig. 5d). This is supported by the observation of a 5-fold higher bias between EC and RS-Met summer daily estimates in those dry years (bias = -0.146 mm d^{-1}), compared to remaining years (bias = -0.029 mm d^{-1}). These negative biases imply an average overestimation by the RS-Met model during the summer compared to observed (EC) ET estimates.

In contrast, the correlation between the RS-Met and EC was high and significant for daily estimates during the rainy season (R=0.80; P<0.0001 for October-May; Fig. 5e). The relatively large discrepancies between RS-Met and EC during the summer indicate the low sensitivity of the RS-Met model to relatively low ET fluxes (i.e., <1.0 mm d^{-1}). This likely suggests the need to adjust the water availability factor (f_{WA}) to positive values for a longer period, particularly at the end of the rainy season-beginning of the summer.

The annual ET, as estimated from both the RS-Met and EC, was higher than the total rainfall amount in some of the years studied (Fig. S3). A similar pattern was previously reported in forests in water-limited regions (Helman et al., 2016; Raz-Yaseef et al., 2012; Williams et al., 2012). ET higher than rainwater supply indicates that trees use water stored in deep soil layers during wet years in the subsequent dry years (e.g., 2006 and 2008; Raz-Yaseef *et al.*, 2012; Barbeta *et al.*, 2015). Thus, the 'transfer' of surplus rainwater from previous years should be also taken into consideration when adjusting the model with available water through the f_{WA} and f_{WD}, which are currently calculated only with the seasonal rainfall. Theoretically, this could be done by summing the available water from the previous year (calculated as P – ET) to the two-month summed P in the calculation of the f_{WA} and f_{WD}. Of course, this would be applied only after completing the ET estimation of the first year.

The adjusted RS-Met GPP (i.e., that with the f_{WD}) was also comparable to the GPP from the EC (765±112 vs. 748±124 g C m^{-2} y^{-1}, for GPP_{MOD} and GPP_{EC}, respectively), and highly correlated at the annual scale (Fig. 6a,b), with an R = 0.91 (P<0.001; N=9) and a low MAE of 52 g C m^{-2} y^{-1} (Relative error of *c.* 7%). MODIS GPP showed inferior correlation with EC estimates at the annual scale, with an R of 0.58 (P=0.08; N=10, Fig. 6c).

6. Testing the RS-Met across a rainfall gradient

Deleted: In general, the interannual trend in ET/P was much
Deleted: noisier
Deleted: when using ET from
Deleted: . This
Deleted: was particularly noted in
Deleted: when the ET from the RS-Met was significantly different from the EC annual estimates (
Deleted: 2004
Deleted: 2006
Deleted: 2010
Deleted: 4a
Deleted: These
Deleted: differences in annual ET most
Deleted: ed
Deleted: from
Deleted: between the two methods
Deleted: r
Deleted:
Deleted: 4c
Deleted: e
Deleted: 2004, 2006 and 2010
Deleted: , which were particularly dry years
Deleted: that from
Deleted: Additionally, t
Deleted: EC
Deleted: r
Deleted:
Deleted: 4d
Deleted: limitation
Deleted: in estimating
Deleted: values
Deleted: in some sites
Deleted: 4a
Deleted: modeled
Deleted: i.e., WS
Deleted: model
Deleted: 5
Deleted: r
Deleted: models

6.1. Comparison with seasonal ET and GPP from EC and MODIS products

We next compared the ET and GPP estimates from the RS-Met model with the field campaign data and MODIS ET/GPP products across the remaining six ecosystems. Comparison between estimates based on the RS-Met model, with and without the f_{WD}, with those from the EC, indicated significantly higher correlations of the adjusted model (i.e., with the f_{WD}) with EC estimates (P=0.06 and P<0.01 for ET and GPP, respectively; Table 2). Only the shrubland site of Kadita showed a higher ET correlation of EC with the unadjusted model. This was likely due to the continuous ET fluxes throughout the summer period in this relatively moist site, which was not captured by the model.

In general, while using the f_{WD} did not improve (for the ET, P>0.1, as indicated by a two-tailed Student's t-test) or only marginally improved (for the GPP, P=0.09, as indicated by a two-tailed Student's t-test) RS-Met estimates in the non-forest sites, it significantly improved the ET and GPP estimates in forest sites (P=0.05 and P=0.016 for ET and GPP, respectively, as indicated by a two-tailed Student's t-test). The adjusted RS-Met successfully tracked changes in ET and CO_2 fluxes from dry to wet season in all sites. Similar to the shown in Yatir, MODIS ET/GPP fluxes were much lower than observed fluxes. This underestimation was particularly noted in the forest sites (Fig. 7 and Fig. S4).

Overall, the adjusted RS-Met was in good agreement with the eddy covariance measurements, with the cross-site regressions producing highly significant linear fits (Fig. 8a, b; R=0.82 and R=0.86; and MAE = 0.47 mm d^{-1} and MAE = 1.89 g C m^{-2} d^{-1} for ET and GPP, respectively). Comparing between the EC *vs.*RS-Met regressions and the EC *vs.* MODIS ET/GPP regressions, using 8-day averaged fluxes values, produced the following linear fits: $ET_{RS\text{-}Met}$ = 1.16 ET_{EC} - 0.11 (R = 0.88; P<0.0001; N = 36) and ET_{MODIS} = 0.38 ET_{EC} + 0.33 (R = 0.65; P<0.0001; N = 33) and $GPP_{RS\text{-}Met}$ = 1.09 GPP_{EC} + 0.21 (R = 0.92; P<0.0001; N = 36) and GPP_{MODIS} = 0.43 GPP_{EC} + 1.31 (R = 0.77; P<0.0001; N = 33), showing a consistent underestimation of both MODIS products (MOD16 and MOD17) in those sites across sites (Fig. 8c,d).

The water-use efficiency (WUE; the slope of the regression between ET and GPP in Fig. S5) was slightly higher at 2.32 g C kg^{-1} H_2O from the RS-Met compared to the low 1.76 g C kg^{-1} H_2O from EC, but it was within the range reported for similar ecosystems in this region (Tang et al., 2014).

6.2. Annual-basis comparisons

Deleted: *daily*
Deleted: (DS)
Deleted: (no-DS)
Deleted: drought stress factor
Deleted: DS
Deleted: s
Deleted: no-DS
Deleted: with the eddy covariance measurements of the ET
Deleted: This likely indicates the sensitivity of the current drought stress factor to local conditions.
Deleted: drought stress factor
Deleted: estimates that included drought stress factor
Deleted: the seasonality
Deleted: of the measured
Deleted: in
Deleted: , though it should be mentioned that the sites of Kadita and Wady Attir had limited measurements to test this (Fig. 6).
Deleted: 7a
Deleted: r
Deleted: r
Deleted: 7c
Deleted: *with ET from PaVI-E*

To expand our analysis across the rainfall gradient, and because we do not have continuous estimations from the EC at the six sites, we compared the annual ET and GPP from the adjusted RS-Met with those from MODIS ET/GPP products. In the case of ET, we also added annual estimates derived from the empirical PaVI-E model (Helman et al. 2015).

The results of our ET comparison showed that the RS-Met and PaVI-E models produced comparable estimates in most of the sites (Fig. 9a), with the only exception being the dryland non-forest site of Wady Attir, which showed higher estimates from RS-Met than from PaVI-E (*P*<0.01, as indicated by Tukey HSD separation procedure). MODIS ET was in accordance with estimates of RS-Met and PaVI-E in shrubland sites in spite of the underestimation of this product during the wet season likely due to the relatively higher ET at the beginning of the rainy season (Fig. 7a). However, MODIS ET was significantly lower than the other two models in the forest sites and also lower than the shrubland sites (Fig. 9a). The cross-site regression between the annual estimates from RS-Met *vs.* those from the EC produced a highly significant linear fit (R=0.94; *P*<0.01), confirming the potential use of the RS-Met in assessing ET at the annual scale across the rainfall gradient in those forest and non-forest sites.

MODIS GPP showed relatively comparable estimates to RS-Met at the annual scale due to its overestimation during the dry season that compensated its underestimation during the peak growth season (Fig. 9b). Here again, though, underestimation was observed in forest sites, particularly in the sites of Eshtaol and Birya.

6.3. Changes in water use efficiency following afforestation across rainfall gradient

We finally used the adjusted RS-Met to assess the impact of afforestation on the water and carbon budgets across the rainfall gradient in Israel by comparing fluxes in the three pine forests (i.e., Yatir, Eshtaol and Birya) with those from the adjacent shrubland sites (i.e., Wady Attir, Modiin and Kadita, respectively). Results showed that the ET significantly increased due to the afforestation of these areas, particularly at the more humid site of Birya (*c.* 53%), but to a lesser extent at the less humid site of Eshtaol (by *c.* 20%) and with almost no change in ET in the dryland site of Yatir (4%). The GPP also significantly increased in those three paired-sites. Overall, afforestation across the rainfall gradient was responsible for a significant increase in the WUE in this region (Fig. 10). Nevertheless, the positive change in the WUE decreased when moving from the dry Yatir-Wady Attir paired site (279 mm y^{-1}) to

Deleted: that
Deleted: retrieved
Deleted: -
Deleted: in these sites
Deleted: 8
Deleted: a Student's *t*-test
Deleted: In the forest sites, annual ET retrieved from RS-Met was generally higher than that derived from PaVI-E, especially in the wetter site of HaSolelim. Nevertheless, t
Deleted: r
Deleted: models
Deleted: 9

the more humid paired-site of Birya-Kadita (766 mm y^{-1}; Fig. 10), strengthening the importance of afforestation efforts in drylands areas.

7. Summary and conclusions

We have tested here a biophysical-based model of ET and CO_2 fluxes driven by satellite-derived vegetation index and meteorological data (RS-Met) and adjusted with a seasonal water deficit factor. The model was validated against direct flux measurements from extensive field campaigns and a fixed Fluxnet station, and compared with MODIS ET/GPP products at seven evergreen forest and adjacent non-forested ecosystem sites along a steep rainfall gradient in the high-energy water-limited Eastern Mediterranean region. Adjusting the model with the water deficit factor generally improved its performance compared to using the model without this factor, particularly in forest sites. The model also outperformed MODIS-based ET/GPP models, which showed generally lower estimates, particularly in the forest sites suggesting that these models might benefit from the inclusion of the water deficit factor.

Our results show the potential use of this simple biophysical remote-sensing-based model in assessing ET and GPP on a daily basis and at a moderate spatial resolution of 250 m, even in high-energy water-limited environments. The addition of a water deficit factor (based on daily rainfall and radiation and/or temperature data alone) in the RS-Met significantly improved its performance in shrublands and especially in forests in this region and might be used in other global models. Nevertheless, careful attention should be paid to adjusting the deficit water factor to local conditions, with their further development particularly required at the end of the rainy season-beginning of the dry period.

Using the RS-Met, we were able to estimate changes in water use efficiency due to afforestation across the rainfall gradient in Israel. Overall, afforestation across our study area was responsible for a significant increase in the WUE. However, the positive change in the WUE decreased when moving from dry (279 mm y^{-1}) to more humid (766 mm y^{-1}) regions, strengthening the importance of drylands afforestation.

Finally, the use of this simple RS-Met approach linked to flexible campaign-based ground validation, as demonstrated in this study, represents a powerful basis for the reliable extension of ET and GPP estimates across spatial and temporal scales in regions with low density of flux stations.

Deleted: 9
Deleted: using
Deleted: and without the inclusion of
Deleted: and water availability
Deleted: s for daily estimations of ET and CO_2 fluxes,
Deleted: validating
Deleted: the model
Deleted: Adding
Deleted: in the RS-Met
Deleted: the
Deleted: use of the
Deleted: s
Deleted: to
Deleted: (based on daily rainfall and radiation and/or temperature data alone)
Deleted: the
Deleted: estimation
Deleted: of these fluxes
Deleted: available and
Deleted: s
Deleted: the

Acknowledgments

David Helman acknowledges personal grants provided by the Bar-Ilan University Presidential Office (Milgat Hanasi), the JNF-Rieger Foundation, USA, and the Hydrological Service of Israel, Water Authority. S. Rohatyn acknowledges scholarships provided by Ronnie Appleby fund, the Advanced School of Environmental Science of the Hebrew University, and the Israel Ministry of Agriculture. We thank E. Ramati for helping with field work and data processing, G. Fratini for helping with EddyPro, and H. Sagi and A. Pelner for technical assistance. We are also grateful to the Meteorological Service of Israel for providing meteorological data and to NASA for making public the MODIS NDVI datasets. This research was partly supported by the Hydrological Service of Israel, Water Authority (Grant No. 4500962964). Flux measurements were made possible through the financial support from the Israel Science Foundation (ISF), Minerva foundation, JNF-KKL, the Hydrological Service of Israel, Water Authority, and C. Wills and R. Lewis program in Environmental Science.

References

Afik, T., 2009. Quantitative estimation of CO2 fluxes in a semi-arid forest and their dependence on climatic factors. Thesis submitted to R.H. Smith Faculty of Agriculture, Food and Environment of Hebrew University, Rehovot, Israel (in Hebrew). Thesis submitted to R.H. Smith Faculty of Agriculture, Food and Environment of Hebrew University, Rehovot, Israel (in Hebrew).

Ahlström, A., Raupach, M.R., Schurgers, G., Smith, B., Arneth, A., Jung, M., Reichstein, M., Canadell, J.G., Friedlingstein, P., Jain, A.K., Kato, E., Poulter, B., Sitch, S., Stocker, B.D., Viovy, N., Wang, Y.P., Wiltshire, A., Zaehle, S., Zeng, N., 2015. The dominant role of semi-arid ecosystems in the trend and variability of the land CO2 sink. Science (80-.). 348, 895–899. doi:10.1126/science.aaa1668

Allen, R.G., Pereira, L.S., Raes, D., 1998. Crop evapotranspiration : guidelines for computing crop water requirements, FAO irrigation and drainage papers;56. FAO, Rome.

Allen, R. G., Pruitt, W. O., Wright, J. L., Howell, T. A., Ventura, F., Snyder, R., Itenfisu, D., Steduto, P., Berengena, J., Yrisarry, J. B., Smith, M., Pereira, L. S., Raes, D., Perrier, A., Alves, I., Walter, I. and Elliott, R.: A recommendation on standardized surface resistance for hourly calculation of reference ETo by the FAO56 Penman-Monteith method, Agric. Water Manag., 81(1), 1–22, doi:http://dx.doi.org/10.1016/j.agwat.2005.03.007, 2006.

Asaf, D., Rotenberg, E., Tatarinov, F., Dicken, U., Montzka, S.A., Yakir, D., 2013. Ecosystem photosynthesis inferred from measurements of carbonyl sulphide flux. Nat. Geosci 6, 186–190.

Aubinet, M., Grelle, A., Ibrom, A., Rannik, S., Moncrieff, J., Foken, T., Kowalski, A.S., Martin, P.H., Berbigier, P., Bernhofer, C., Clement, R., Elbers, J.A., Granier, A., Grünwald, T., Morgenstern, K., Pilegaard, K., Rebmann, C., Snijders, W., Valentini, R., Vesa, T., 2000. Estimates of the annual net carbon and water exchange of forests: the EUROFLUX methodology. Adv. Ecol. Res. 30, 113–175.

Baldocchi, D.D., 2003. Assessing the eddy covariance technique for evaluating carbon dioxide exchange rates of ecosystems: past, present and future. Glob. Chang. Biol. 9, 479–492.

Barbeta, A., Mejía-Chang, M., Ogaya, R., Voltas, J., Dawson, T.E., Peñuelas, J., 2015. The combined effects of a long-term experimental drought and an extreme drought on the use of plant-water sources in a Mediterranean forest. Glob. Chang. Biol. 21, 1213–1225. doi:10.1111/gcb.12785

Ciais, P., Reichstein, M., Viovy, N., Granier, a, Ogée, J., Allard, V., Aubinet, M., Buchmann, N., Bernhofer, C., Carrara, a, Chevallier, F., De Noblet, N., Friend, a D., Friedlingstein, P., Grünwald, T., Heinesch, B., Keronen, P., Knohl, a, Krinner, G., Loustau, D., Manca, G., Matteucci, G., Miglietta, F., Ourcival, J.M., Papale, D., Pilegaard, K., Rambal, S., Seufert, G., Soussana, J.F., Sanz, M.J., Schulze, E.D., Vesala, T., Valentini, R., 2005. Europe-wide reduction in primary productivity caused by the heat and drought in 2003. Nature 437, 529–533. doi:10.1038/nature03972

Cleveland, W.S., 1979. Robust locally weighted regression and smoothing scatterplots. J. Am. Stat. Assoc. 74, 829–836.

Gamon, J.A., Field, C.B., Goulden, M.L., Griffin, K.L., Hartley, A.E., Joel, G., Peñuelas, J., Valentini, R., 1995. Relationships between NDVI, canopy structure, and photosynthesis in three Californian vegetation types. Ecol. Appl. 28–41.

Garbulsky, M.F., Filella, I., Verger, a., Peñuelas, J., 2014. Photosynthetic light use efficiency from satellite sensors: From global to Mediterranean vegetation. Environ. Exp. Bot. 103, 3–11. doi:10.1016/j.envexpbot.2013.10.009

Garbulsky, M.F., Penuelas, J., Papale, D., Filella, I., 2008. Remote estimation of carbon dioxide uptake by a Mediterranean forest. Glob. Chang. Biol. 14, 2860–2867. doi:10.1111/j.1365-2486.2008.01684.x

Glenn, E., Nagler, P., Huete, A., 2010. Vegetation Index Methods for Estimating Evapotranspiration by Remote Sensing. Surv. Geophys. 31, 531–555. doi:10.1007/s10712-010-9102-2

Glenn, E.P., Huete, A.R., Nagler, P.L., Nelson, S.G., 2008. Relationship Between Remotely-sensed Vegetation Indices, Canopy Attributes and Plant Physiological Processes: What Vegetation Indices Can and Cannot Tell Us About the Landscape. Sensors 8, 2136–2160. doi:10.3390/s8042136

Glenn, E.P., Neale, C.M.U., Hunsaker, D.J., Nagler, P.L., 2011. Vegetation index-based crop coefficients to estimate evapotranspiration by remote sensing in agricultural and natural ecosystems. Hydrol. Process. 25, 4050–4062. doi:10.1002/hyp.8392

Helman, D., (under review). Land Surface Phenology: What do we really 'see' from space?

Helman, D., Givati, A., Lensky, I.M., 2015a. Annual evapotranspiration retrieved from satellite vegetation indices for the eastern Mediterranean at 250 m spatial resolution. Atmos. Chem. Phys. 15, 12567–12579. doi:doi:10.5194/acp-15-12567-2015

Helman, D., Lensky, I.M., Mussery, A., Leu, S., 2014a. Rehabilitating degraded drylands by creating woodland islets: Assessing long-term effects on aboveground productivity and soil fertility. Agric. For. Meteorol. doi:10.1016/j.agrformet.2014.05.003

Helman, D., Lensky, I.M., Tessler, N., Osem, Y., 2015b. A phenology-based method for monitoring woody and herbaceous vegetation in Mediterranean forests from NDVI time series. Remote Sens. 7, 12314–12335. doi:10.3390/rs70912314

Helman, D., Lensky, I.M., Yakir, D., Osem, Y., 2016. Forests growing under dry conditions have higher hydrological resilience to drought than do more humid forests. Glob. Chang. Biol. doi:10.1111/gcb.13551

Helman, D., Leu, S., Mussery, A., (under review) Contrasting effects of two *Acacia* species on understorey growth in a drylands environment: Interplay of water and light availability.

Helman, D., Mussery, A., Lensky, I.M., Leu, S., 2014b. Detecting changes in biomass productivity in a different land management regimes in drylands using satellite-derived vegetation index. Soil Use Manag. 30, 32–39. doi:10.1111/sum.12099

Helman, D., Osem, Y., Yakir, D., Lensky, I.M., 2017. Relationships between climate, topography, water use and productivity in two key Mediterranean forest types with different water-use strategies. Agric. For. Meteorol. 232, 319–330. doi:http://dx.doi.org/10.1016/j.agrformet.2016.08.018

Huete, A., Didan, K., Miura, T., Rodriguez, E.P., Gao, X., Ferreira, L.G., 2002. Overview of the radiometric and biophysical performance of the MODIS vegetation indices. Remote Sens. Environ. 83, 195–213.

Jensen, M.E., Haise, H.R., 1963. Estimating evapotranspiration from solar radiation. Proc. Am. Soc. Civ. Eng. J. Irrig. Drain. Div. 89, 15–41.

Jung, M., Reichstein, M., Ciais, P., Seneviratne, S.I., Sheffield, J., Goulden, M.L., Bonan, G., Cescatti, A., Chen, J., de Jeu, R., Dolman, A.J., Eugster, W., Gerten, D., Gianelle, D., Gobron, N., Heinke, J., Kimball, J., Law, B.E., Montagnani, L., Mu, Q., Mueller, B., Oleson, K., Papale, D., Richardson, A.D., Roupsard, O., Running, S., Tomelleri, E., Viovy, N., Weber, U., Williams, C., Wood, E., Zaehle, S., Zhang, K., 2010. Recent decline in the global land evapotranspiration trend due to limited moisture supply. Nature 467, 951–954. doi:10.1038/nature09396

Kalma, J., McVicar, T., McCabe, M., 2008. Estimating Land Surface Evaporation: A Review of Methods Using Remotely Sensed Surface Temperature Data. Surv. Geophys. 29, 421–469. doi:10.1007/s10712-008-9037-z

Klein, T., Rotenberg, E., Tatarinov, F., Yakir, D., 2016. Association between sap flow-derived and eddy covariance-derived measurements of forest canopy CO2 uptake. New Phytol. 209, 436–446. doi:10.1111/nph.13597

Klein, T., Shpringer, I., Fikler, B., Elbaz, G., Cohen, S., Yakir, D., 2013. Relationships between stomatal regulation, water-use, and water-use efficiency of two coexisting key Mediterranean tree species. For. Ecol. Manage. 302, 34–42.

Kool, D., Agam, N., Lazarovitch, N., Heitman, J.L., Sauer, T.J., Ben-Gal, a., 2014. A review of approaches for evapotranspiration partitioning. Agric. For. Meteorol. 184, 56–70. doi:10.1016/j.agrformet.2013.09.003

Llusia, J., Roahtyn, S., Yakir, D., Rotenberg, E., Seco, R., Guenther, A., Peñuelas, J., 2016. Photosynthesis, stomatal conductance and terpene emission response to water availability in dry and mesic Mediterranean forests. Trees 30, 749–759. doi:10.1007/s00468-015-1317-x

Ma, X., Huete, A., Yu, Q., Restrepo-Coupe, N., Beringer, J., Hutley, L.B., Kanniah, K.D., Cleverly, J., Eamus, D., 2014. Parameterization of an ecosystem light-use-efficiency model for predicting savanna GPP using MODIS EVI. Remote Sens. Environ. 154, 253–271. doi:10.1016/j.rse.2014.08.025

Maselli, F., Barbati, A., Chiesi, M., Chirici, G., Corona, P., 2006. Use of remotely sensed and ancillary data for estimating forest gross primary productivity in Italy. Remote Sens. Environ. 100, 563–575. doi:10.1016/j.rse.2005.11.010

Maselli, F., Papale, D., Chiesi, M., Matteucci, G., Angeli, L., Raschi, A., Seufert, G., 2014. Operational monitoring of daily evapotranspiration by the combination of MODIS NDVI and ground meteorological data: Application and evaluation in Central Italy. Remote Sens. Environ. 152, 279–290. doi:10.1016/j.rse.2014.06.021

Maselli, F., Papale, D., Puletti, N., Chirici, G., Corona, P., 2009. Combining remote sensing and ancillary data to monitor the gross productivity of water-limited forest ecosystems. Remote Sens. Environ. 113, 657–667. doi:10.1016/j.rse.2008.11.008

Maseyk, K., Hemming, D., Angert, A., Leavitt, S.W., Yakir, D., 2011. Increase in water-use efficiency and underlying processes in pine forests across a precipitation gradient in the dry Mediterranean region over the past 30 years. Oecologia 167, 573–585. doi:10.1007/s00442-011-2010-4

Maseyk, K.S., Lin, T., Rotenberg, E., Grünzweig, J.M., Schwartz, A., Yakir, D., 2008. Physiology-phenology interactions in a productive semi-arid pine forest. New Phytol. 178, 603–616.

Monteith, J.L., 1977. Climate and the efficiency of crop production in Britain. Phil. Trans. R. Soc. Lond. B 281, 277–294.

Mu, Q., Heinsch, F. A., Zhao, M. and Running, S. W.: Development of a global evapotranspiration algorithm based on MODIS and global meteorology data, Remote Sens. Environ., 111, 519–536, doi:10.1016/j.rse.2006.07.007, 2007.

Mu, Q., Zhao, M. and Running, S. W.: Improvements to a MODIS global terrestrial evapotranspiration algorithm, Remote Sens. Environ., 115(8), 1781–1800, doi:10.1016/j.rse.2011.02.019, 2011.

Mussery, A., Helman, D., Leu, S., Budovsky, A., 2016. Modeling herbaceous productivity considering tree-grass interactions in drylands savannah: The case study of Yatir farm in the Negev drylands. J. Arid Environ. 124, 160–164. doi:10.1016/j.jaridenv.2015.08.013

Myneni, R.B., Williams, D.L., 1994. On the relationship between FAPAR and NDVI. Remote Sens. Environ. 49, 200–211. doi:10.1016/0034-4257(94)90016-7

Nagaraja Rao, C.R., 1984. Photosynthetically active components of global solar radiation: Measurements and model computations. Arch. Meteorol. Geophys. Bioclimatol. Ser. B 34, 353–364. doi:10.1007/BF02269448

Osem, Y., Zangy, E., Bney-Moshe, E., Moshe, Y., 2012. Understory woody vegetation in manmade Mediterranean pine forests: variation in community structure along a rainfall gradient. Eur. J. For. Res. 131, 693–704. doi:10.1007/s10342-011-0542-0

Peñuelas, J., Garbulsky, M.F., Filella, I., 2011. Photochemical reflectance index (PRI) and remote sensing of plant CO_2 uptake. New Phytol. 191, 596–9. doi:10.1111/j.1469-8137.2011.03791.x

Raz-Yaseef, N., Yakir, D., Schiller, G., Cohen, S., 2012. Dynamics of evapotranspiration partitioning in a semi-arid forest as affected by temporal rainfall patterns. Agric. For. Meteorol. 157, 77–85. doi:10.1016/j.agrformet.2012.01.015

Reichstein, M., Bahn, M., Ciais, P., Frank, D., Mahecha, M.D., Seneviratne, S.I., Zscheischler, J., Beer, C., Buchmann, N., Frank, D.C., Papale, D., Rammig, A., Smith, P., Thonicke, K., Velde, M. van der, Vicca, S., Walz, A., Wattenbach, M., 2013. Climate extremes and the carbon cycle. Nature 500, 287–295. doi:10.1038/nature12350

Reichstein, M., Falge, E., Baldocchi, D., Papale, D., Aubinet, M., Berbigier, P., Bernhofer, C., Buchmann, N., Gilmanov, T., Granier, A., Grünwald, T., Havránková, K., Ilvesniemi, H., Janous, D., Knohl, A., Laurila, T., Lohila, A., Loustau, D., Matteucci, G., Meyers, T., Miglietta, F., Ourcival, J.-M., Pumpanen, J., Rambal, S., Rotenberg, E., Sanz, M., Tenhunen, J., Seufert, G., Vaccari, F., Vesala, T., Yakir, D., Valentini, R., 2005. On the separation of net ecosystem exchange into assimilation and ecosystem respiration: review and improved algorithm. Glob. Chang. Biol. 11, 1424–1439. doi:10.1111/j.1365-2486.2005.001002.x

Rotenberg, E., Yakir, D., 2011. Distinct patterns of changes in surface energy budget associated with forestation in the semiarid region. Glob. Chang. Biol. 17, 1536–1548. doi:10.1111/j.1365-2486.2010.02320.x

Running, S.W., Nemani, R.R., 1988. Relating seasonal patterns of the AVHRR vegetation index to simulated photosynthesis and transpiration of forests in different climates. Remote Sens. Environ. 24, 347–367. doi:10.1016/0034-4257(88)90034-X

Running, S.W., Nemani, R.R., Heinsch, F.A., Zhao, M., Reeves, M., Hashimoto, H., 2004. A Continuous Satellite-Derived Measure of Global Terrestrial Primary Production. Bioscience 54, 547–560. doi:10.1641/0006-3568(2004)054[0547:ACSMOG]2.0.CO;2

Running, S.W., Thornton, P.E., Nemani, R., Glassy, J.M., 2000. Global Terrestrial Gross and Net Primary Productivity from the Earth Observing System, in: Methods in Ecosystem Science. Ed. O E Sala, R B Jackson, H A Mooney, and R W Howarth, pp. 44–57.

Schimel, D., Pavlick, R., Fisher, J.B., Asner, G.P., Saatchi, S., Townsend, P., Miller, C., Frankenberg, C., Hibbard, K., Cox, P., 2015. Observing terrestrial ecosystems and the carbon cycle from space. Glob. Chang. Biol. 21, 1762–1776. doi:10.1111/gcb.12822

Sims, D.A., Rahman, A.F., Cordova, V.D., El-Masri, B.Z., Baldocchi, D.D., Bolstad, P. V, Flanagan, L.B., Goldstein, A.H., Hollinger, D.Y., Misson, L., Monson, R.K., Oechel, W.C., Schmid, H.P., Wofsy, S.C., Xu, L., 2008. A new model of gross primary productivity for North American ecosystems based solely on the enhanced vegetation index and land surface temperature from MODIS. Remote Sens. Data Assim. Spec. Issue 112, 1633–1646. doi:10.1016/j.rse.2007.08.004

Sprintsin, M., Cohen, S., Maseyk, K., Rotenberg, E., Grünzweig, J., Karnieli, a., Berliner, P., Yakir, D., 2011. Long term and seasonal courses of leaf area index in a semi-arid forest plantation. Agric. For. Meteorol. 151, 565–574. doi:10.1016/j.agrformet.2011.01.001

Tang, X., Li, H., Desai, A.R., Nagy, Z., Luo, J., Kolb, T.E., Olioso, A., Xu, X., Yao, L., Kutsch, W., Pilegaard, K., Köstner, B., Ammann, C., 2014. How is water-use efficiency of terrestrial ecosystems distributed and changing on Earth? Sci. Rep. 4, 7483. doi:10.1038/srep07483

Tatarinov, F., Rotenberg, E., Maseyk, K., Ogée, J., Klein, T., Yakir, D., 2016. Resilience to seasonal heat wave episodes in a Mediterranean pine forest. New Phytol. 210, 485–496. doi:10.1111/nph.13791

Turner, D. P., Ritts, W. D., Cohen, W. B., Maeirsperger, T. K., Gower, S. T., Kirschbaum, A. A., Running, S. W., Zhao, M., Wofsy, S. C., Dunn, A. L., Law, B. E., Campbell, J. L., Oechel, W. C., Kwon, H. J., Meyers, T. P., Small, E. E., Kurc, S. A. and Gamon, J. A.: Site-level evaluation of satellite-based global terrestrial gross primary production and net primary production monitoring, Glob. Chang. Biol., 11(4), 666–684, doi:10.1111/j.1365-2486.2005.00936.x, 2005.

Veroustraete, F., Sabbe, H., Eerens, H., 2002. Estimation of carbon mass fluxes over Europe using the C-Fix model and Euroflux data. Remote Sens. Environ. 83, 376–399. https://doi.org/10.1016/j.ecolmodel.2006.06.008

Wang, H., Zhao, P., Zou, L.L., McCarthy, H.R., Zeng, X.P., Ni, G.Y., Rao, X.Q., 2014. CO2 uptake of a mature Acacia mangium plantation estimated from sap flow measurements and stable carbon isotope discrimination. Biogeosciences 11, 1393–1411. doi:10.5194/bg-11-1393-2014

Way, D. a., Oren, R., Kroner, Y., 2015. The space-time continuum: the effects of elevated CO2 and temperature on trees and the importance of scaling. Plant. Cell Environ. 38, 991–1007. doi:10.1111/pce.12527

Williams, C.A., Reichstein, M., Buchmann, N., Baldocchi, D., Beer, C., Schwalm, C., Wohlfahrt, G., Hasler, N., Bernhofer, C., Foken, T., Papale, D., Schymanski, S., Schaefer, K., 2012. Climate and vegetation controls on the surface water balance: Synthesis of evapotranspiration measured across a global network of flux towers. Water Resour. Res. 48. doi:10.1029/2011WR011586

Wu, C., Huang, W., Yang, Q., Xie, Q., 2015. Improved estimation of light use efficiency by removal of canopy structural effect from the photochemical reflectance index (PRI). Agric. Ecosyst. Environ. 199, 333–338. doi:10.1016/j.agee.2014.10.017

Zhao, M., Running, S.W., 2010. Drought-Induced Reduction in Global Terrestrial Net

Primary Production from 2000 Through 2009. Science (80-.). 329, 940–943.

Tables

Table 1. Site characteristics and locations divided into two groups of forest (top) and non-forest (bottom) sites. In each group, sites are arranged from the dry to the humid (from top to bottom).

Site	Location (Lat, N; Lon, E)	PFT	Dominant species	Grazing	Altitude	P	AF
Yatir	31.3451; 35.0519	CF	*P. halepensis*	sheep	660	279	0.19
Eshtaol	31.7953; 34.9954	CF	*P. halepensis*	sheep	385	480	0.34
HaSolelim	32.7464; 35.2317	OF	*Q. ithaburensis*	cattle	180	543	0.42
Birya	33.0015; 35.4823	CF	*P. halepensis*	cattle	750	766	0.63
Wady Attir	31.3308; 34.9905	SH	*Phagnalon rupestre*	sheep	490	279	0.11
Modiin	31.8698; 35.0125	SH	*S. spinosum*	cattle	245	480	0.32
Kadita	33.0110; 35.4614	SH	*S. spinosum*	cattle	815	766	0.63

PFT is the plant functional type (CF, Coniferous forest; OF, oak forest; SH, shrubland); Grazing indicates the main grazing regime in the site; altitude is in meters above sea level; P is the mean annual rainfall (mm y^{-1}); and AF is the aridity factor calculated as the P to the ET_o ratio (in mm mm^{-1}).

Table 2. Statistics of the comparison between the RS-Met with the addition of the water deficit factor (f_{WD}) and without its addition (NO f_{WD}) and the eddy covariance-derived measurements.

	ET (mm d^{-1})					GPP (g C m^{-1} d^{-1})				
	N	Correlation		MAE		N	Correlation		MAE	
		NO f_{WD}	f_{WD}	NO f_{WD}	f_{WD}		NO f_{WD}	f_{WD}	NO f_{WD}	f_{WD}
Yatir	2228	0.05*	**0.76**	1.9	0.18	2293	0.56	**0.77**	1.3	0.8
Eshtaol	47	0.16ns	**0.64**	1.3	1.6	54	0.80	**0.90**	2.3	2.3
HaSolelim	40	0.72	**0.79**	2.0	0.8	41	0.80	**0.88**	2.1	2.1
Birya	57	0.72	**0.85**	1.8	1.8	57	0.64	**0.72**	4	3
Wady Attir	28	0.80	**0.91**	0.5	0.7	29	0.90	**0.92**	0.7	1.0
Modiin	43	0.62	**0.64**	1.9	1.0	43	0.89	**0.90**	1.2	1.2
Kadita	28	**0.80**	0.67	0.8	1.0	28	0.82	**0.88**	1.8	1.8

The mean absolute error (MAE) is in mm d^{-1} for the ET and in g C m^{-2} d^{-1} for the GPP. All the correlations were highly statistically significant at P<0.001, except for the ET model without the f_{WD} at the forest site of Yatir (*) that was significant at P=0.02, and the site of Eshtaol that was not statistically significant (ns). The number of days used for the correlation in each site and flux is indicated (N=days).

Figures

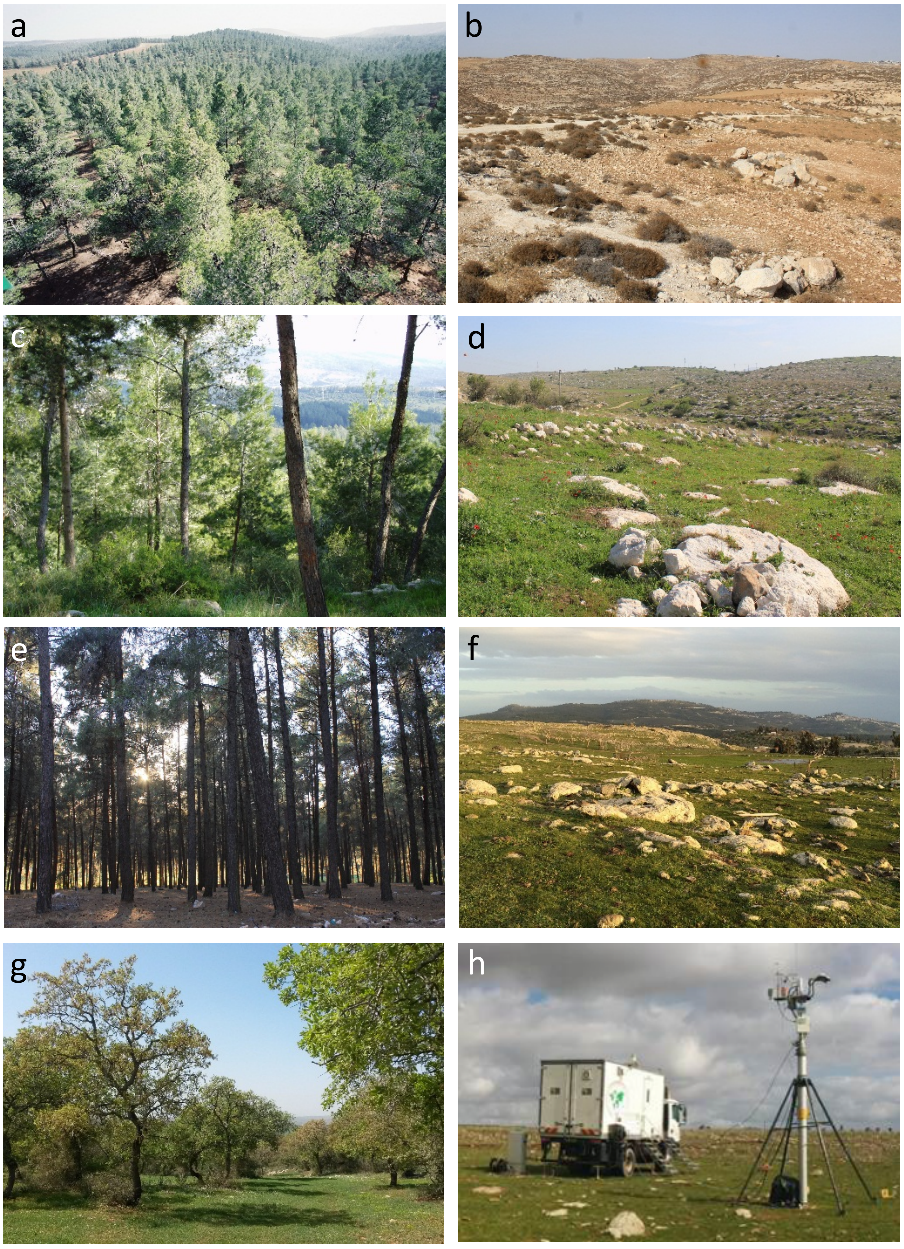

Fig. 1. Views of the seven study sites along the climatic gradient **(a – g)** and the newly mobile flux measurement system used in this study **(h)**. Sites include three paired of planted pine forests (*Pinus halepensis*) and adjacent non-forest sites (representing the original environment on which these forests were planted): Yatir **(a)** and Wady Attir **(b)**; Eshtaol **(c)** and Modiin **(d)**; Birya **(e)** and Kadita **(f)**. The deciduous oak forest of HaSolelim is shown **(d)**. The three paired sites **(a-f)** represent the geo-climatic transition from xeric to mesic environments in Israel, respectively.

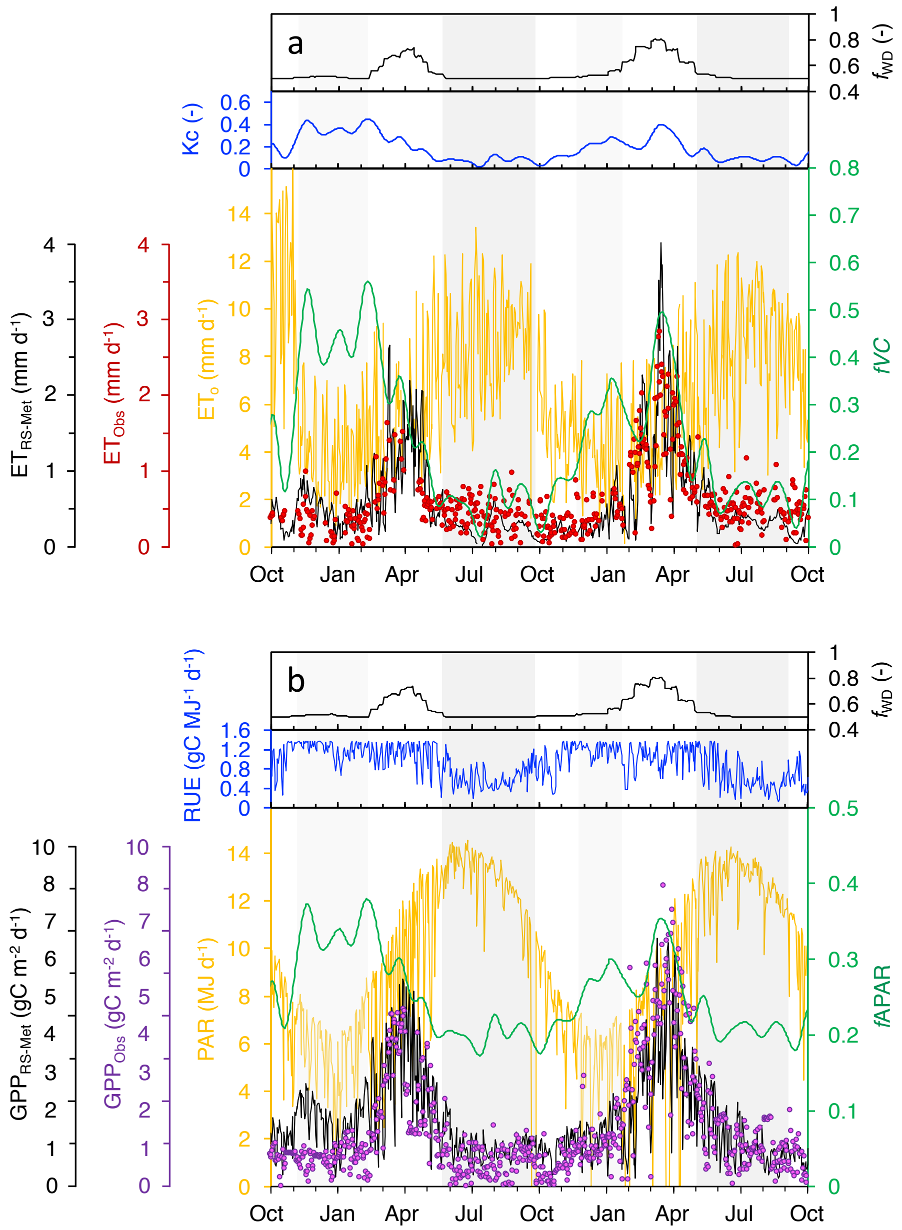

Fig. 2. Seasonal evolution of the water deficit factor (f_{WD}; black line in upper panel) and the main drivers of the modeled ET **(a)** and GPP **(b)** at the semiarid pine forest of Yatir ($ET_{RS\text{-}Met}$ and $GPP_{RS\text{-}Met}$, respectively; black line in lower panel) for the seasonal years 2008/9 and 2009/10. EC fluxes are also shown (ET_{Obs} and GPP_{Obs}, red and purple dots, respectively). The K_C and the radiation use efficiency (RUE) both without the addition of the f_{WD} (blue in middle panels) are shown together with the potential ET (ET_o; yellow in **a**), the fraction of vegetation cover (*fVC*; green in **a**), the photosynthetic active radiation (PAR; yellow in **b**), and the fraction of absorbed PAR (*f*APAR; green in **b**). Colored vertical bands indicate the critical periods when the addition of f_{WD} is particularly useful.

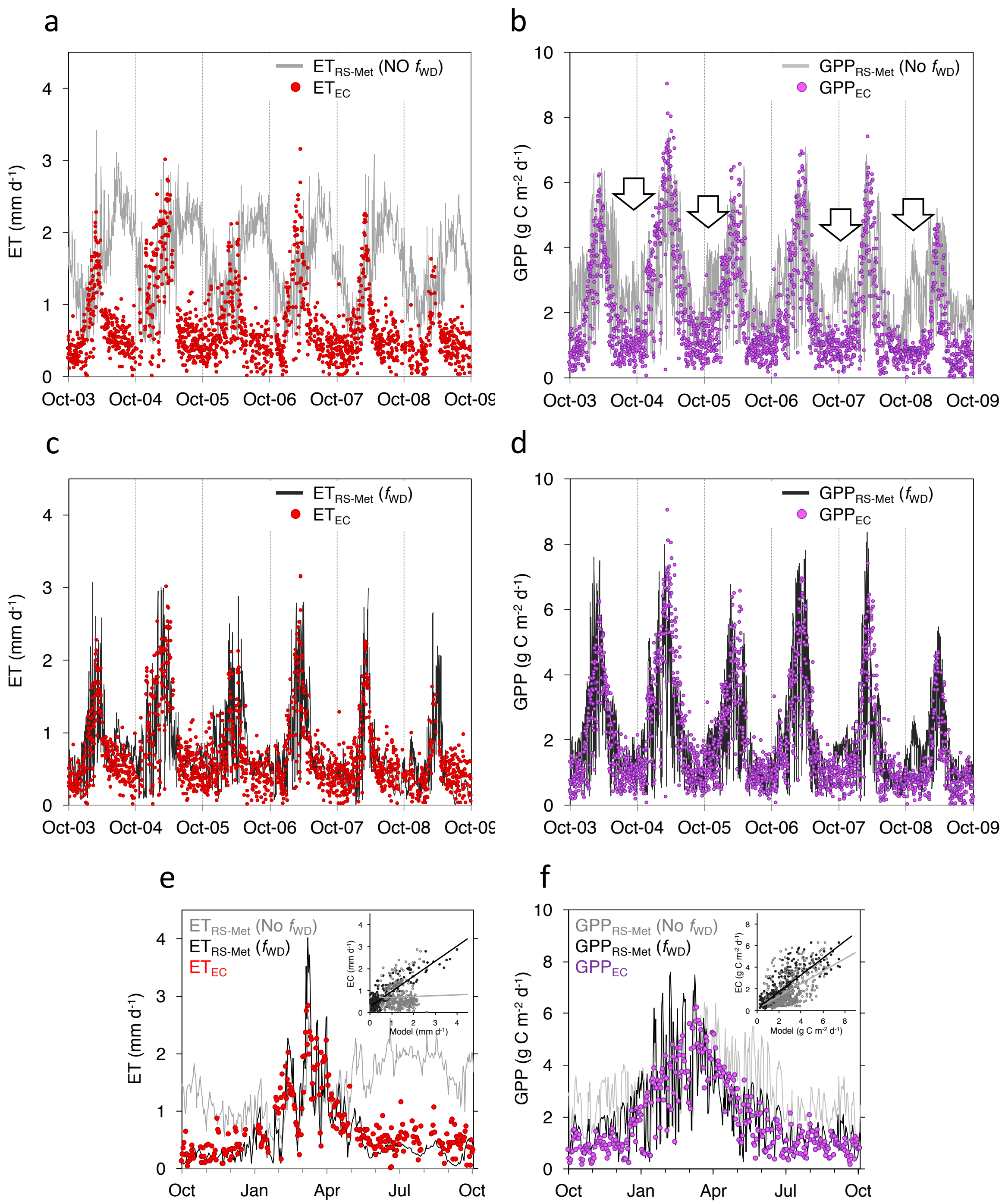

Fig. 3. Observed (EC) and modeled (RS-Met) ET and GPP at Yatir. Shown in **(a – d)** are the RS-Met with (black) and without (grey) the water deficit factor (f_{WD}). Closer look at selected years 2009/10 and 2003/4 are shown in **(e)** and **(f)**, respectively. Inserts show the correlations between modeled and observed fluxes with and without the f_{WD} (black and grey dots, respectively).

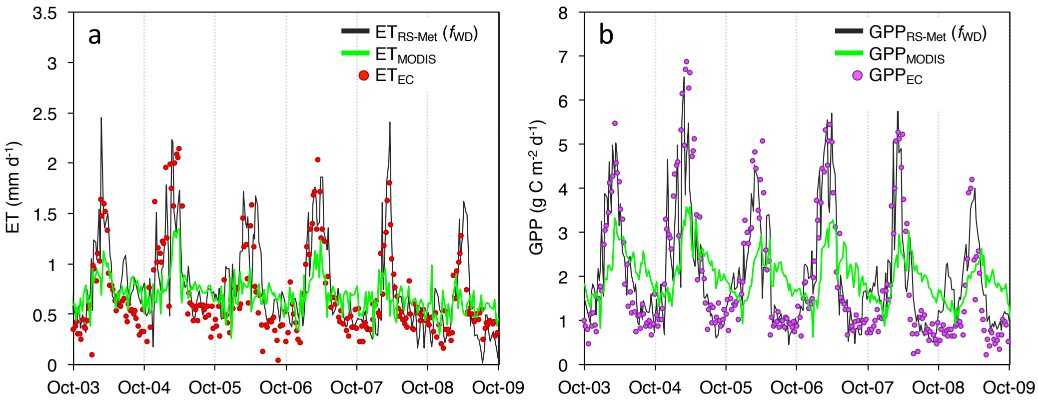

Fig. 4. Eight-day averaged values of ET **(a)** and GPP **(b)** from EC (dots), RS-Met (black) and MODIS (green) at Yatir. The R of the correlation for EC *vs.* RS-Met is 0.78 and 0.80 for ET and GPP, respectively (slope = 0.90 and 0.70; intercept = 0.19 and 0.66 for ET and GPP, respectively). The R of the correlation for EC *vs.* MODIS is 0.47 and 0.60 for ET and GPP, respectively (slope = 0.21 and 0.27; intercept = 0.56 and 1.47 for ET and GPP, respectively).

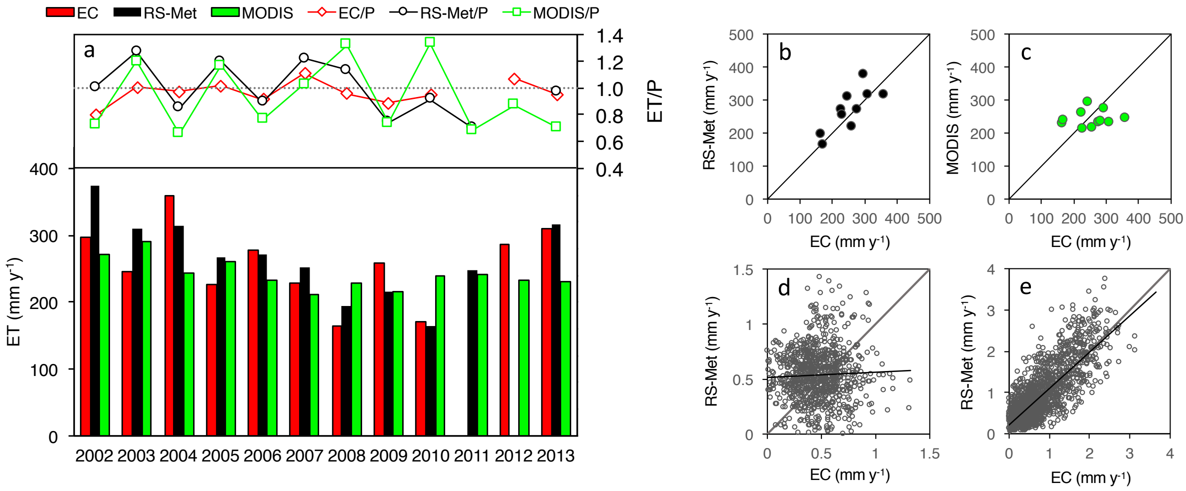

Fig. 5. Annual ET (mm y^{-1}) summed from daily RS-Met (with f_{WD}; black), MODIS (green) and EC (red) at Yatir forest site for 2003-2014 **(a)**. Linear regressions of the EC *vs.* RS-Met **(b)** and EC *vs.* MODIS **(c)**. Daily estimates from RS-Met in dry summer (June-August; **d**) and rainy (October-May; **e**) seasons. The R's of the linear fits for EC *vs.* RS-Met **(b)** and MODIS **(c)** are 0.78 (P<0.05; N=10) and 0.10 (P>0.1; N=11), respectively. The R's of the linear fits for the daily data in **(d)** and **(e)** are 0.05 (P>0.1; N=876) and 0.80 (P<0.0001; N=1570), respectively. The interannual trends in ET/P from EC, RS-Met and MODIS are presented in the upper panel of **(a)**. Note that the annual sums of ET from EC and RS-Met in 2012 and 2013, respectively, are not displayed due to the scarcity of available data during these years (>50% missing data).

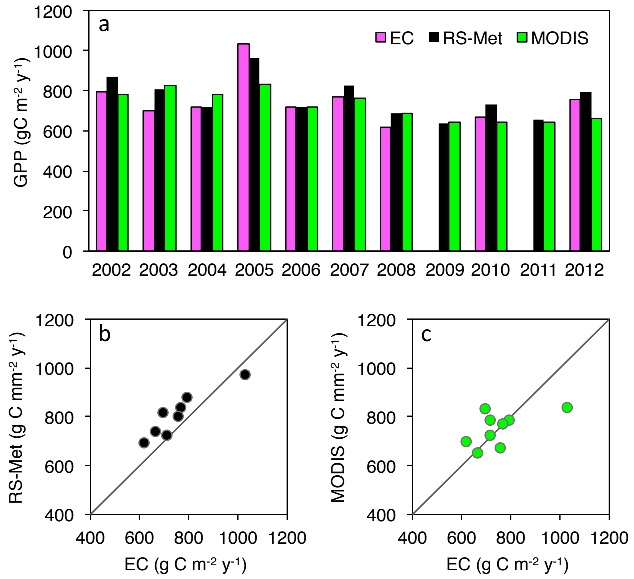

Fig. 6. Annual GPP sums (g C m^{-2} y^{-1}) from EC, RS-Met (with f_{WD}) and the 8-day MOD16 product (MODIS) at Yatir **(a);** and the linear regressions of EC vs. RS-Met **(b)** and MODIS **(c)**. The R of the linear fits is 0.91 ($P<0.05$; N=10) and 0.58 ($P=0.08$; N=10) for RS-Met and MODIS, respectively. Annual EC GPP for 2009 and 2011 were not calculated due to missing data.

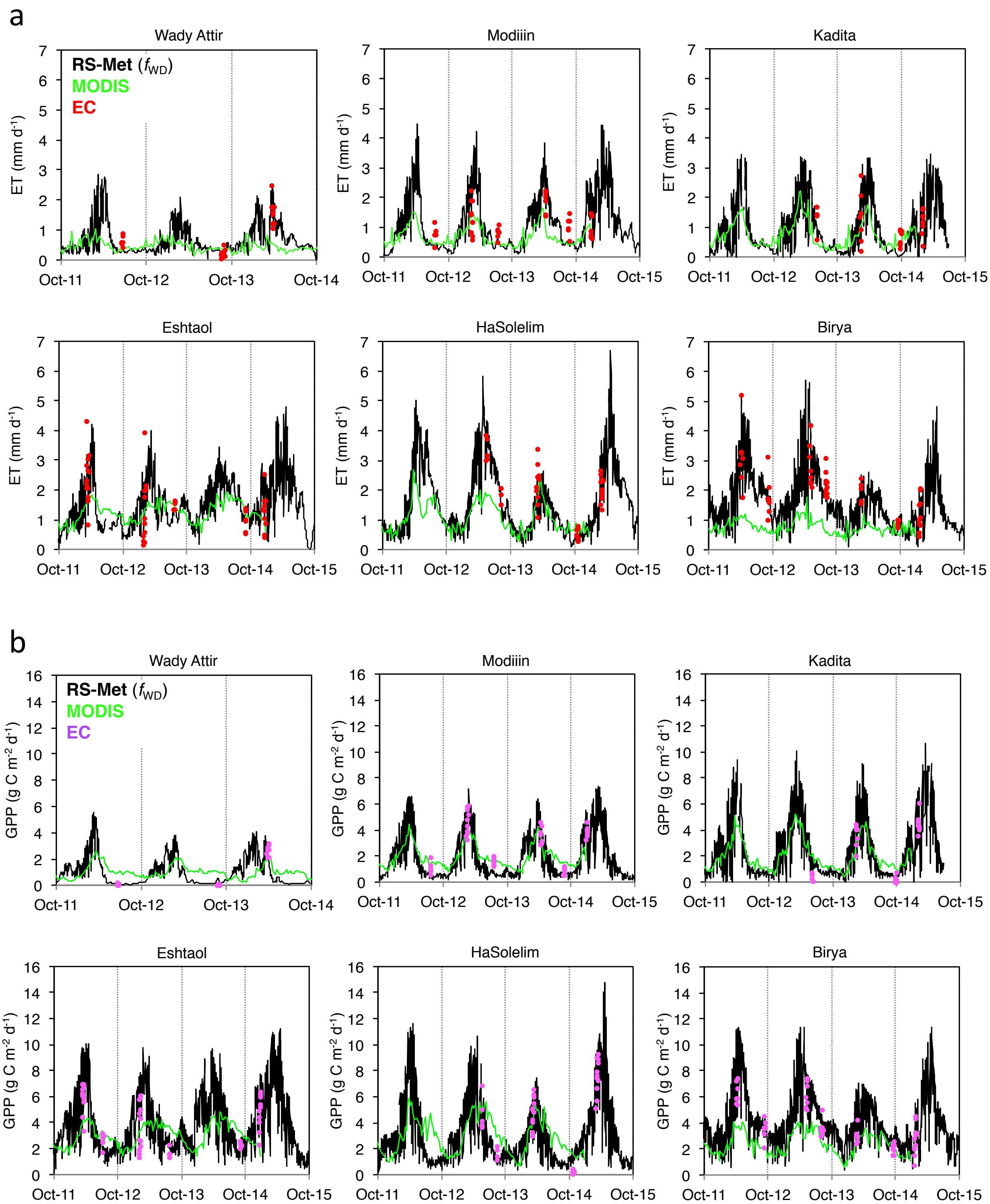

Fig. 7. ET **(a)** and GPP **(b)** from EC, RS-Met (with f_{WD}) and MODIS (MOD16A2 and MOD17A2 products, respectively) at the six forest and non-forested sites.

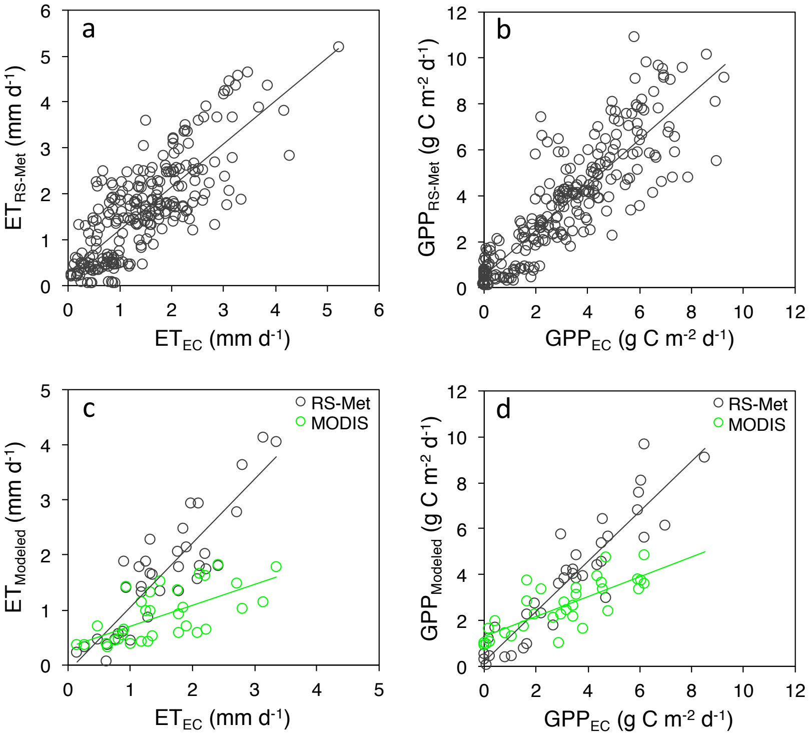

Fig. 8. Cross-site EC *vs.* model correlations of ET **(a, c)** and GPP **(b, d)**. In **(a)** and **(b)** are the EC *vs.* RS-Met (with f_{WD}) using all EC data from the six sites (each dot representing a single date), with linear fits of $ET_{RS\text{-}Met} = 0.936\ ET_{EC} + 0.281$ (R = 0.82; P<0.0001; N = 243) and $GPP_{RS\text{-}Met} = 0.990\ GPP_{EC} + 0.515$ (R = 0.86; P<0.0001; N = 252) for ET and GPP, respectively. In **(c)** and **(d)** are the same cross-site correlations but with data averaged over 8-day periods for comparisons with MODIS ET and GPP products (8-day averaged values). Linear fits for EC *vs.* RS-Met and MODIS in **(c)** are $ET_{RS\text{-}Met} = 1.16\ ET_{EC} - 0.11$ (R = 0.88; P<0.0001; N = 36) and $ET_{MODIS} = 0.38\ ET_{EC} + 0.33$ (R = 0.65; P<0.0001; N = 33), respectively. In **(d)**, linear fits are $GPP_{RS\text{-}Met} = 1.09\ GPP_{EC} + 0.21$ (R = 0.92; P<0.0001; N = 36) and $GPP_{MODIS} = 0.43\ GPP_{EC} + 1.31$ (R = 0.77; P<0.0001; N = 33) for EC *vs.* RS-Met and MODIS, respectively.

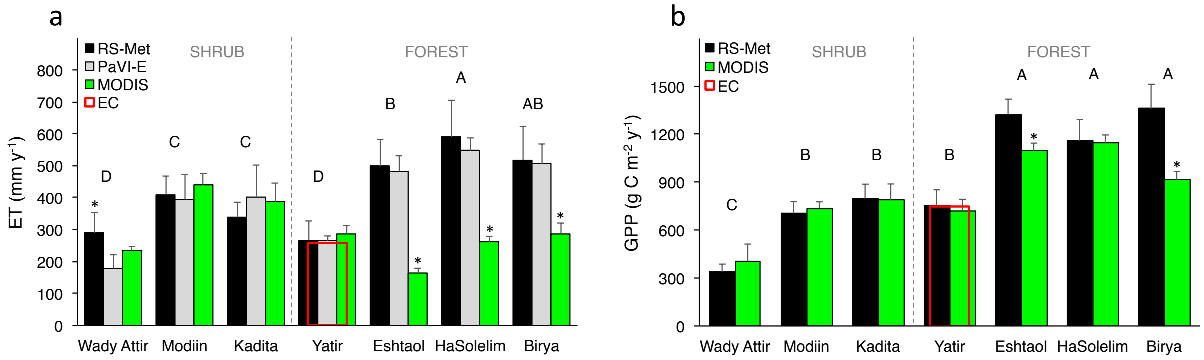

Fig. 9. Mean annual (2003-2013) estimates of ET **(a)** and GPP **(b)** from RS-Met (black), MODIS (green) and PaVI-E (grey; only for ET in **a**; Helman *et al.*, 2015a) at the seven sites. *Uppercase* letters indicate significant differences at P<0.05 between sites from Tukey HSD separation procedure following two-way ANOVA for the interaction of site × model (using PaVI-E and RS-Met in **a** and MODIS and RS-Met in **b**). Asterisks indicate significant different values from other models for the specific site, as indicated by Tukey HSD. The EC annual sums at Yatir are also shown (red).

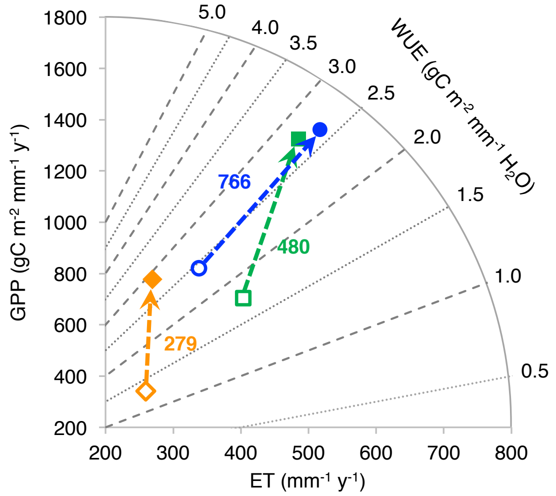

Fig. 10. The change in GPP, ET and water use efficiency (WUE; as indicated by the direction of the arrow) attributed to the afforestation (closed symbols) of shrubland areas (open symbols) across a rainfall gradient in Israel (279-766 mm y^{-1}). The three-paired forest and non-forest sites of Yatir-Wady Attir, Eshtaol-Modiin and Birya-Kadita are indicated with yellow, green and blue colors, respectively. The rainfall level at each paired site is indicated near the arrow (in mm y^{-1}). Note the changing slope of the change in ET and GPP, indicating that the gain in WUE due to afforestation decreases from dry to humid areas.

Supplement of

A remote sensing-based biophysical model for daily estimations of evapotranspiration and CO_2 uptake in high-energy water-limited environments

D. Helman *et al.*

Correspondence to: D. Helman (davidhelman.biu@gmail.com)

Figures

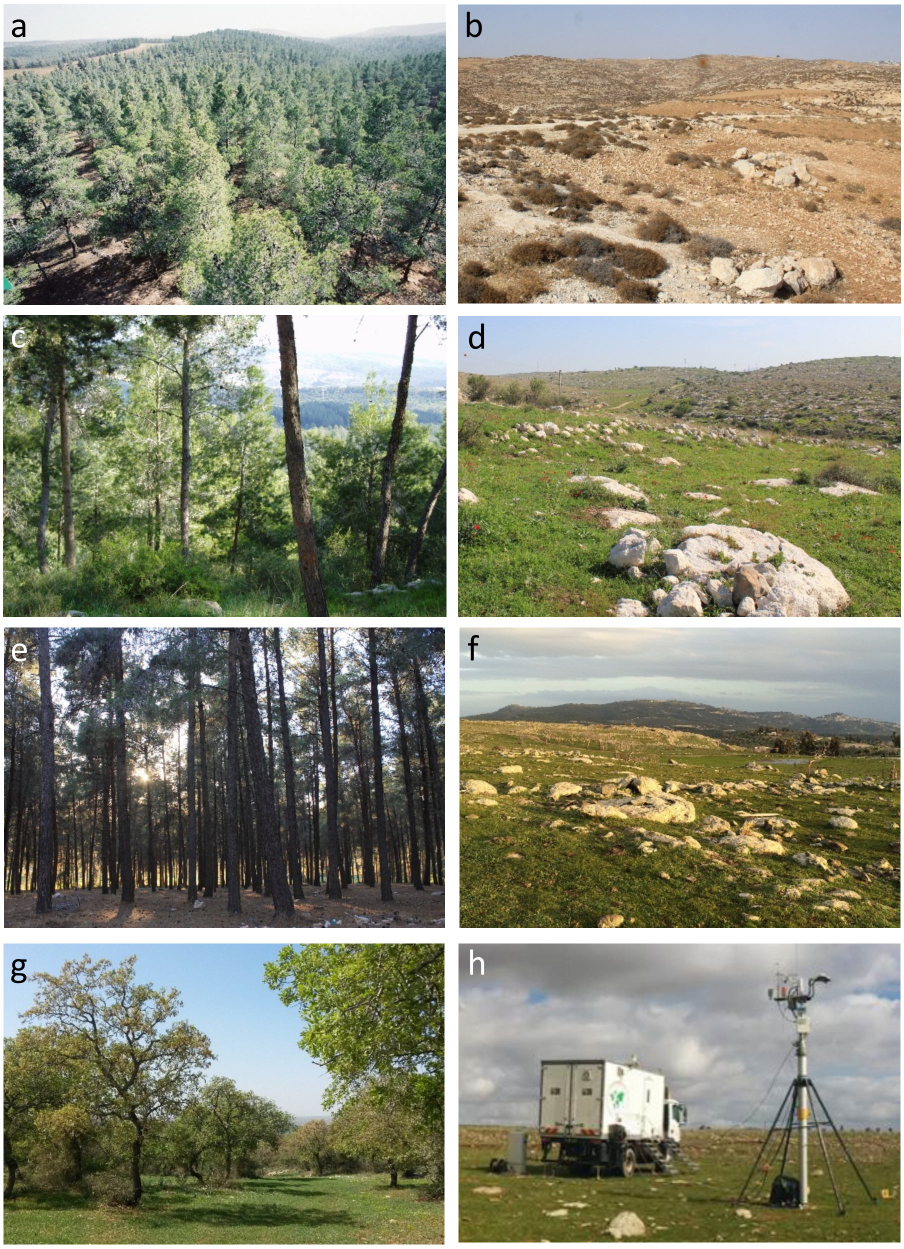

Fig. S1. Views of the seven study sites along the climatic gradient **(a – g)** and the newly mobile flux measurement system used in this study **(h)**. This figure is the same as Fig. 1 in main article.

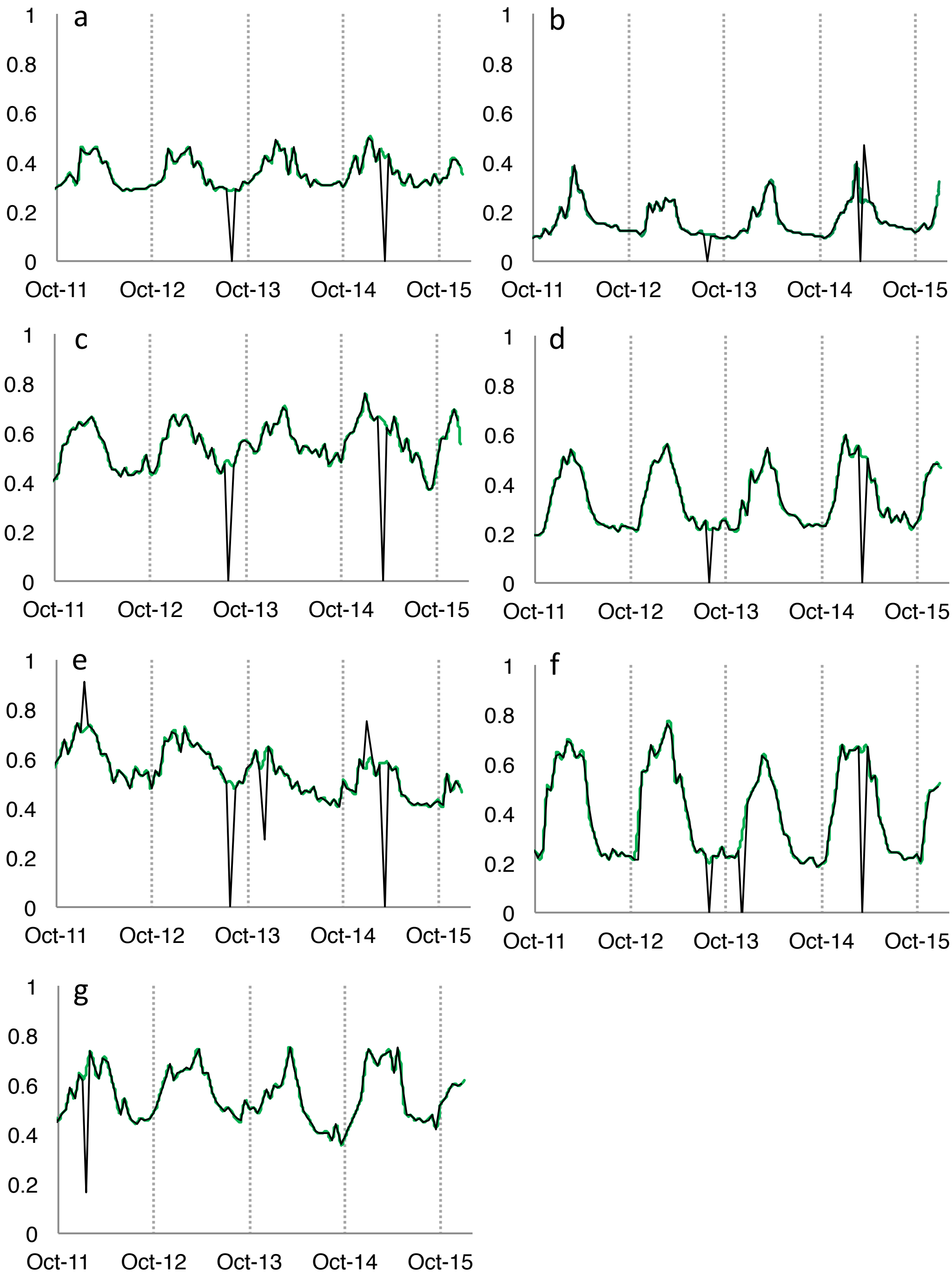

Fig. S2. Original (black line) and smoothed (green line) time series of NDVI (MOD13Q1) in the seven sites (see sites in Fig. S1 and respective locations in Table 1 in the main article). Smoothing and interpolation of the 16-day data to daily values was achieved using local weighted scatterplot smoothing technique (LOESS). The elimination of outliers by LOESS is clearly seen in the time series of all sites.

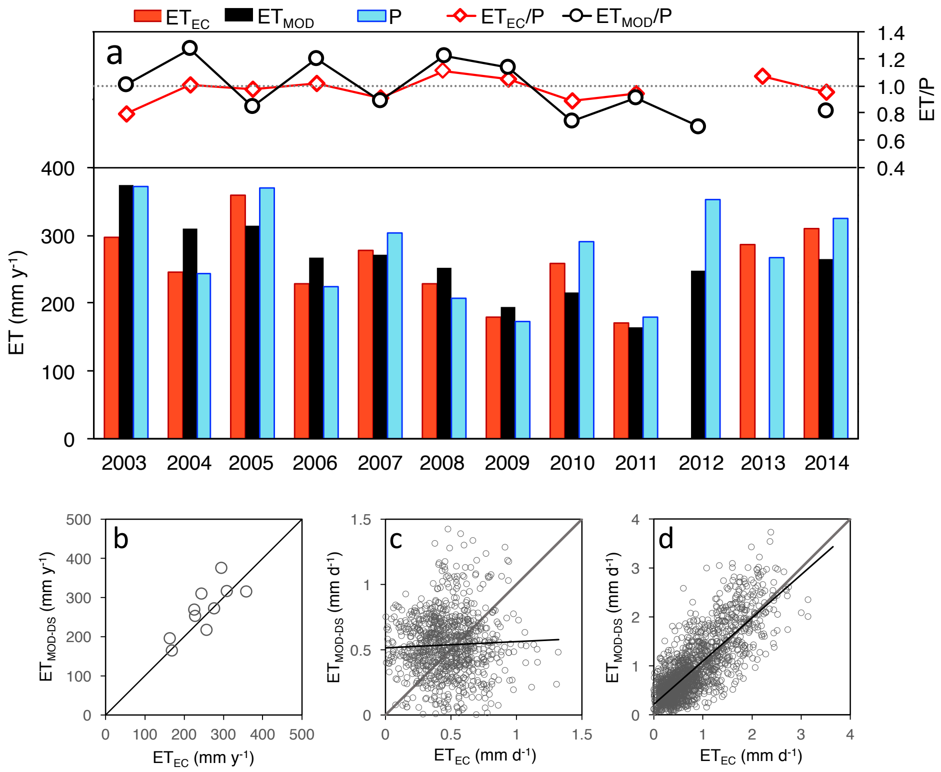

Fig. S3. Annual ET (mm y^{-1}) summed from daily RS-Met estimates (with f_{WD}) and EC, and annual rainfall amounts (P) at Yatir pine forest site for 2003-2014 **(a)**. Linear EC *vs.* RS-Met ET regressions of the annual **(b)** and daily estimates during dry summer (June-August; **c**) and rainy (October-May; **d**) seasons. The R's of the linear fits are 0.78 (P<0.05; N=10) in **(b)**, 0.05 (P>0.1; N=876) in **(c)** and 0.80 (P<0.0001; N=1570) in **(d)**. The interannual trends in ET/P from EC and RS-Met are presented in upper panel of **(a)**. Note that annual sums of ET from EC and RS-Met in 2012 and 2013, respectively, are not displayed due to the scarcity of available data during these years (>50% missing data).

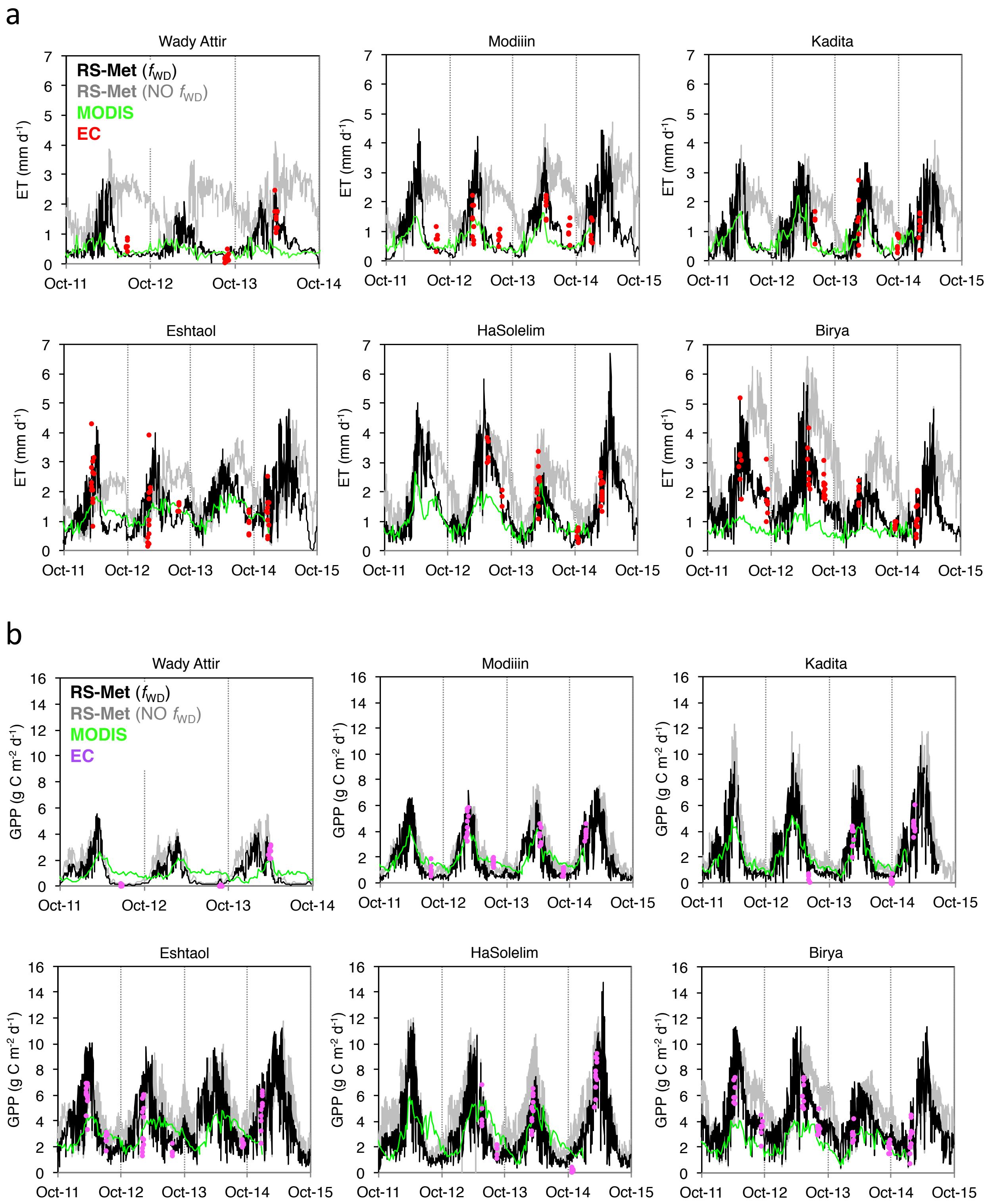

Fig. S4. Same as Fig. 7 in main article with the addition of RS-Met without the f_{WD} (grey line).

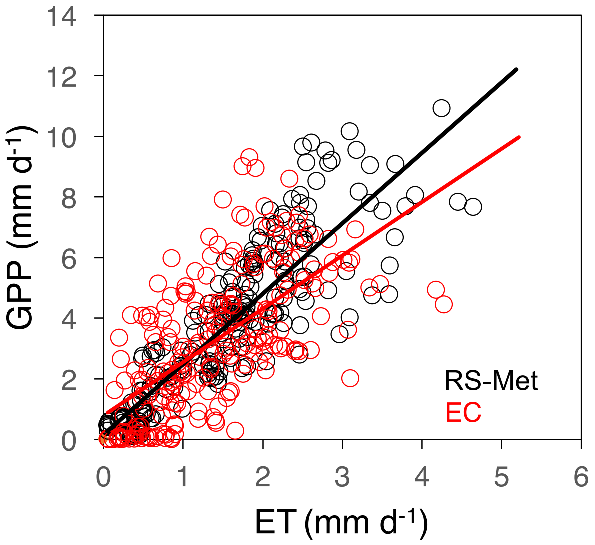

Fig. S5. Cross-site correlations between eddy ET and GPP from EC (red) and RS-Met (black). The RS-Met with the water deficit factor (f_{WD}) is shown. The slopes of the linear fits in are 2.32 g C kg^{-1} H_2O and 1.76 g C kg^{-1} H_2O for RS-Met and EC, with R = 0.87 and 0.65 (P<0.0001; N = 243 for both), respectively.